Final Report

NASA Grant NAG 3-393

NASA Lewis Research Center

entitled

Investigation of Surface Tension Driven Convection as a Feasibility Study for a Micro-Gravity Experiment

E. L. Koschmieder

submitted to

Grant Office
Nasa Lewis Research Center
Cleveland, Ohio

March 1988

I. Introduction

We shall provide first a review of the basic problem that was addressed in the work done for the feasibility study of a micro-gravity surface tension driven convection experiment. The origin of the surface tension driven convection problem is a classic paper of Benard (1900) about cellular convection in a shallow fluid layer. The fundamental discovery of this study were the hexagonal convection cells, which are now referred to as the Benard cells. A sample of hexagonal cells is shown in Fig. 1.

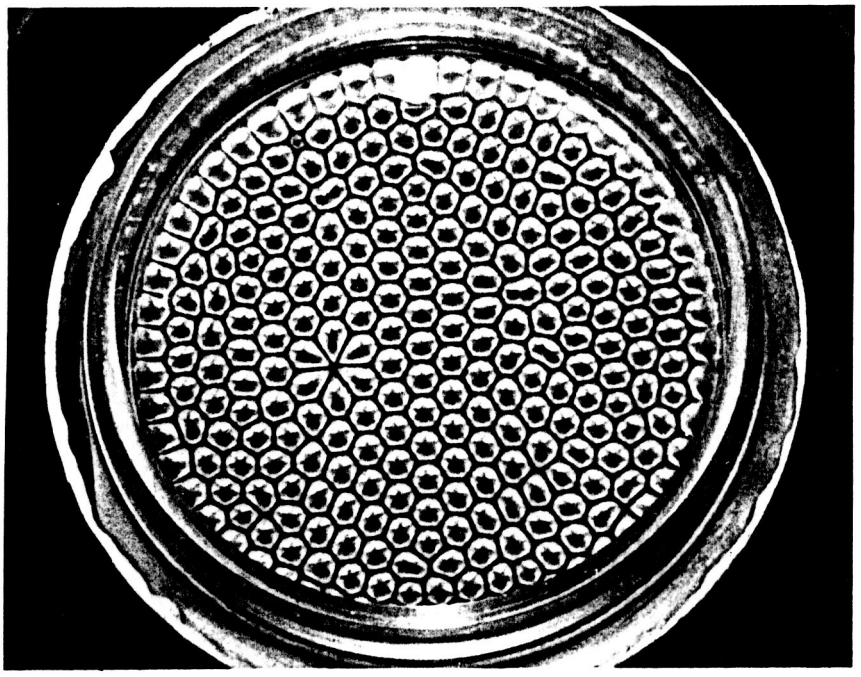

Hexagonal Benard cells. After Koschmieder (1974)

The pioneering theoretical work dealing (supposedly) with the explanation of the Benard cells was Rayleigh's (1916) theory about the stability of a fluid layer heated uniformly from below. A truely classical paper. It concerns the most simple stability problem in Fluid Mechanics, namely the stability of a fluid layer which is initially at rest. The investigation of Benard convection and Rayleigh's theory were believed to deal with the same problem until 1956, when in a one page paper Block showed experimentally that surface tension effects must play a fundamental role in the formation of the Benard cells. Independently it was shown theoretically by Pearson (1958) that surface tension gradients alone are able to create an instability in a resting fluid, and that thereby hexagonal cells can be formed.

The most interesting feature of Pearson's theory in the context of our feasibility study is that Pearson postulated that gravity is zero. Nevertheless the hexagonal cells are a solution of his theory, which is linear, hence mathematically unambiguous but not strictly verifiable in a laboratory on Earth. It is, however, nowadays accepted as a fact that surface tension is the driving force in the formation of the hexagonal convection cells, and not buoyancy, as it originally followed from Rayleigh's theory. Since surface tension can be easily eliminated in a convection experiment by putting a lid into contact with the fluid, the Rayleigh problem has remained a fundamental problem in Hydrodynamic Stability, it has now, however, a parallel, Pearsons's problem.

The amount of experimental work on surface tension driven Benard convection (Pearson's problem) was very limited when our feasibility study began. There was one paper dealing with the size (or the so-called wavelength) of the hexagonal cells by Koschmieder (1967) and one paper by Palmer and Berg (1971) on the measurement of the critical Marangoni number required to be reached for onset of surface tension driven convection. There was also an attempt to observe the onset of surface tension driven convection in microgravity on board of the Apollo 14 and 17 space flights, (Grodzka and Bannister 1972, 1975). I have served as a scientific consultant for these experiments. In spite of the determined and admirable efforts of the astronauts these experiments are considered to be inconclusive.

2. The feasibility studies.

When I made my first proposal to NASA Lewis concerning a microgravity surface tension driven convection experiment two items were foremost on my mind. First that we had to make first of all a good laboratory test of the consequences of surface tension gradients on the onset of convection in a laboratory on Earth, and second that we had to learn about surface tension driven convection in small containers, because this configuration was likely to be the way a convection experiment in space had to be made.

Concerning item #1 the following: It was known from a theoretical study of Nield (1968) how gravity interacts with surface tension to cause the onset of convection in shallow fluid layers on Earth. It was argued by some that the results of Nield's theory permitted experiments in a laboratory on Earth which would approximate with sufficient accuracy the results of Pearson's theory, if only the fluid layer was sufficiently thin. Although this argument was not convincing, the only way to settle this matter was by an experiment. Our first effort was therefore the investigation of the onset of convection in thin fluid layers of large lateral extent (or aspect ratio). The results of our

experiments are described in the paper of Koschmieder and Biggerstaff (1986), see appendix 1. It would be senseless to repeat here the details. I will, however, state our basic result. We have learned that it is not possible to approximate the results of Pearson's theory by running convection experiments in very thin fluid layers in the presence of gravity. The reason for our finding is the occurrence of a subcritical instability. This means that in very thin fluid layers of depth of about 1 mm (or less) motions form in the fluid at Marangoni numbers below the critical Marangoni number predicted by Pearson. The thinner the layer is, the earlier the subcritical motions appear, contradicting flatly the expected behavior. That is not a fault of Pearson's theory, rather a consequence of the attempt to create (via a thin fluid layer) conditions which approximate Pearsons's theory. There are not shortcuts, if one wants to verify Pearsons's theory unambiguously one has to do that with zero g (or its approximation microgravity). In microgravity there is no need to use thin fluid layers to approximate Pearsons's theory, actually the experimental difficulties increase as the fluid depth decreases.

The subcritical instability that we discovered in our experiments was theoretically unexpected and not welcome with some of my colleagues, although the evidence is quite clear, the subcritical motions can be seen with the naked eye, see figures 2a-c in appendix 1. We were already engaged in experiments with small containers when it occurred to me that there is a way to run a critical test on the reality of the subcritical instability. This can be done by checking for subcritical motions in thin fluid layers in buoyancy driven convection, or Rayleigh-Benard convection as it is called. We have, therefore, interrupted our experiments with small containers and made a crash effort with Rayleigh-Benard convection in thin fluid layer, a topic never investigated before. The results of this effort are described in appendix 2. This manuscript has be submitted for publication to the Journal of Fluid Mechanics. We will not present here the details of this paper either. The basic result is quite simple. A subcritical instability occurs in Rayleigh-Benard convection as well, if the fluid layer is sufficiently thin. As it turned out, the subcritical instability is a principal feature of onset of convection in very thin fluid layers, regardless whether the instability is surface-tension driven or buoyancy driven. If one does not work with thin fluid layers the subcritical instability does not occur, buoyancy driven experiments provide correct results, and surface tension driven experiments should provide correct results, if the acceleration of gravity is eliminated.

Having completed this study we returned to surface tension driven convection in small containers. This problem had been studied theoretically by Rosenblat, Davis, and Homsy (1982 a,b). The patterns found in our study for various aspect ratios in one

and the same either circular or square container are shown in figures 2 and 3.

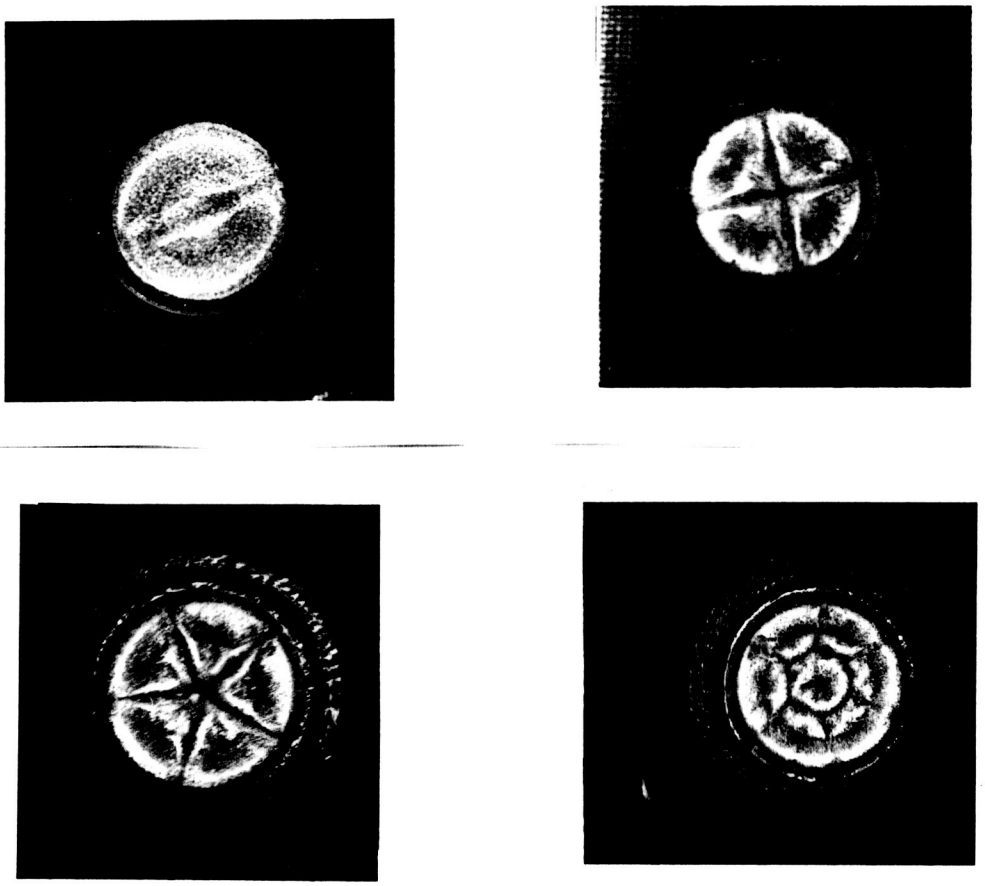

Fig. 2

While the patterns in the circular container conform with expectations, the patterns found in the square container are quite original. The fluid has found surprising ways to pack either two or three square cells or e.g. six square cells. It is, of course, natural to pack a square container with either one or four square cells, and the fluid readily does so. The patterns shown here are startling examples of the effect lateral boundaries can have on pattern formation. doing such experiments in microgravity will only enhance the clarity of the results, because microgravity will reduce the thermal effects the lateral boundaries might have on the out come of these experiments. The last experiment on this topic was made on Aug 20, 1987, our financial support ended on February 28, 1987. Due to other pressing commitments the paper describing these experiments has not yet been written, but is on my agenda for this spring semester.

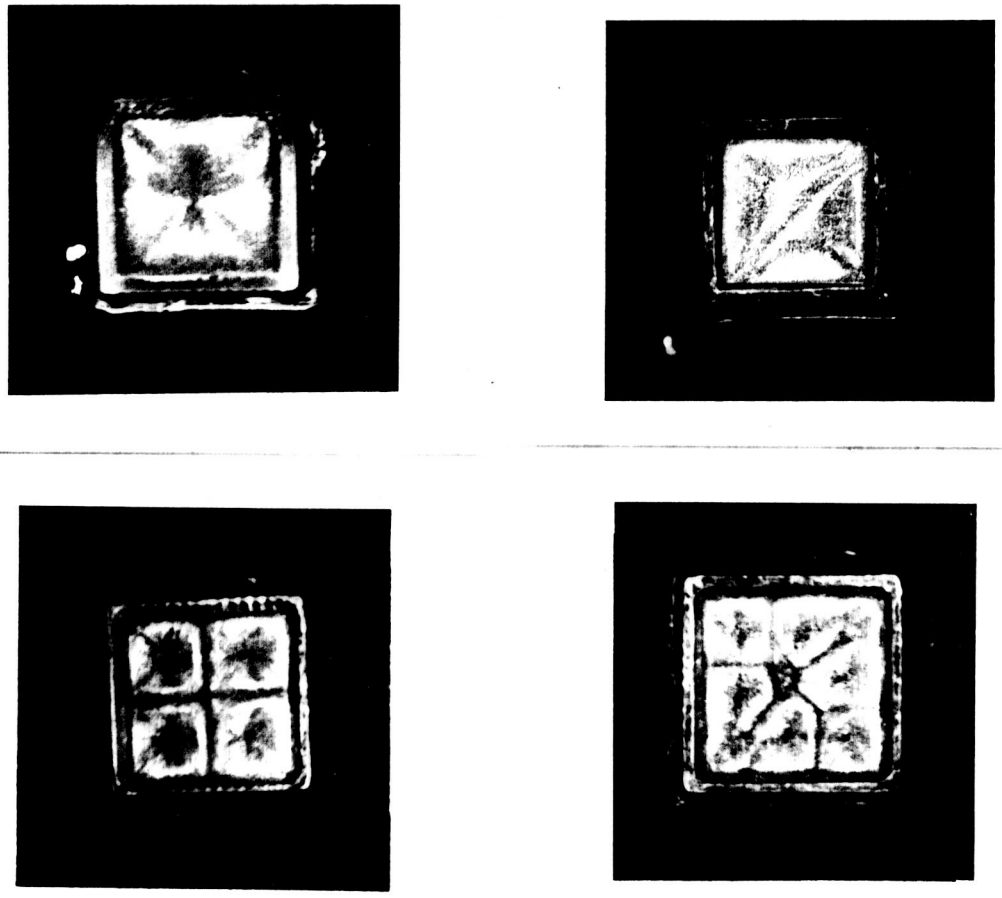

Fig. 3

I would finally, like to express my sincere appreciation to NASA for the interest in and support of this work. It was as a a matter of fact, on several occasions exciting to pursue these investigations.

J. Fluid Mech. (1986), *vol.* 167, *pp.* 49–64
Printed in Great Britain

Onset of surface-tension-driven Bénard convection

By E. L. KOSCHMIEDER AND M. I. BIGGERSTAFF

College of Engineering and I. Prigogine Center for Statistical Mechanics,
The University of Texas, Austin, TX 78712, USA

(Received 4 April 1985 and in revised form 20 November 1985)

An experimental investigation of the onset of convection in shallow fluid layers heated uniformly from below and cooled from above by an air layer has been made. If the depth of the silicone layer is smaller than 2 mm the onset of convection takes place in two stages. There is first a weak pattern, which is characterized by its appearance at ever smaller temperature gradients as the depth of the fluid is decreased. When the temperature difference across the fluid is increased a second strong pattern forms near the predicted critical Marangoni number. The cells in this pattern are hexagonal and seem to be what one has always referred to as Bénard cells. The temperature gradient at which this pattern appears increases with decreased depth. The heat transfer through the fluid has been measured. The critical temperature gradient for the formation of the hexagonal pattern has been determined from the break of the heat transfer curve.

1. Introduction

The investigations of Bénard (1900) marked the beginning of the study of fluid motions in a shallow fluid layer heated uniformly from below. The most notable observation of Bénard was the hexagonal convection cells, now commonly referred to as Bénard cells. Today, 86 years later, we still do not possess a convincing explanation for the formation of the hexagonal cells, and for the preference for hexagonal cells over the other possible cellular patterns.

Rayleigh's (1916) pioneering theoretical analysis of the stability of a layer of fluid heated from below seemed to provide a basis for the understanding of the Bénard cells. Rayleigh's most fundamental result however was the discovery of the existence of a critical or minimal temperature gradient required for the onset of convection. Bénard had not noticed the existence of such a critical gradient in his experiments. Actually, in a later evaluation of his experiments (Bénard 1930), he came to the conclusion that he had observed convection at temperature differences about 10^{-4} to 10^{-5} times smaller than the critical temperature gradient predicted by Rayleigh. Bénard's interpretation of his own experiments was ignored. We shall see in the following that his interpretation of his experiments was correct.

A new aspect was introduced into the explanation of the Bénard cells by Block (1956). He concluded from his experiments that surface tension must play a significant role in the formation of the hexagonal cells. He also pointed out that convective motions occurred at temperature differences of a fraction of the predicted critical value. A short time thereafter the same points were established theoretically by Pearson (1958). Pearson, who investigated surface forces only, showed that the onset of surface-tension-driven convection is determined by the critical value of a non-dimensional parameter, the Marangoni number. From the value of the critical

Marangoni number, and from the linear dependence of the Marangoni number on the depth of the fluid it follows that the onset of convection in shallow fluid layers should occur at critical temperature differences much smaller than those predicted by Rayleigh's theory. An explanation for the discrepancies of the experimental and theoretical values of the critical temperature difference had apparently been found. However, we will show in the following that the onset of surface-tension-driven convection occurs at temperature differences significantly below those predicted by the critical Marangoni number.

Pearson's theory has been augmented by the studies of Nield (1964), and Scriven & Sternling (1964). Nield studied the conditions for the onset of surface-tension-driven convection in the presence of gravity, i.e. he dealt with the situation experienced in the laboratory and obviously present in Bénard's experiments. He found that surface-tension-driven convection and buoyancy-driven convection are coupled. In the case of very shallow fluid layers the minimal temperature difference required for the onset of convection in the presence of gravity is, according to Nield, determined by the critical Marangoni number. Scriven & Sternling neglect gravity, just as Pearson did, but take various other parameters into account, in particular the surface tension coefficient S, not only the variation of surface tension with temperature dS/dT, in which form surface tension appears in the Marangoni number. Smith (1966) extended these two studies by considering the effect of gravity waves. He found that surface waves are usually important only for very small wavenumbers.

The results of Scriven & Sternling differ drastically from those of Pearson as well as Nield. They find that onset of convection in very shallow fluid layers can occur at very small temperature differences, the onset temperature difference decreasing with decreased fluid depth. This differs clearly from the result to be expected when either the critical Marangoni number or the critical Rayleigh number determine the onset of motion. An onset of convection governed by, for example, the critical Marangoni number implies that the critical temperature gradient increases as the depth of the fluid is decreased. As will be shown in the following, the onset of convection with a free (air) surface actually occurs at smaller temperature differences if the fluid depth is decreased, provided that the depth of the fluid is smaller than a certain value above which the conventional critical Marangoni number determines the onset of motion.

The stability of a non-deformable fluid layer subject to buoyancy and surface-tension forces has been investigated with the energy method by Davis (1969). Davis finds a subcritical instability in a small range of Marangoni numbers for sufficiently small Rayleigh numbers. These energy method studies have been confirmed by Davis & Homsy (1980) with an investigation of the same problem but with a deformable surface. Castillo & Velarde (1982) have studied, also with the energy method, the stability of two-component or one-component fluid layers with a deformable surface heated from below or from above, and found likewise this subcritical instability.

Nonlinear theoretical studies of surface-tension-driven convection have been made by Scanlon & Segel (1967), Kraska & Sani (1979), and Cloot & Lebon (1984), all trying to explain the preference for the hexagonal cells. Recently Rosenblat, Davis & Homsy (1982*a*, *b*) have investigated surface-tension-driven convection in bounded circular or rectangular fluid layers of small aspect ratio. There are only two modern experimental investigations of surface-tension-driven Bénard convection. Koschmieder (1967) observed the formation of a regular hexagonal cell pattern and determined the wavelength of the convective motions. Palmer & Berg (1971) determined the critical Marangoni number from the break of the heat transfer curve which is caused

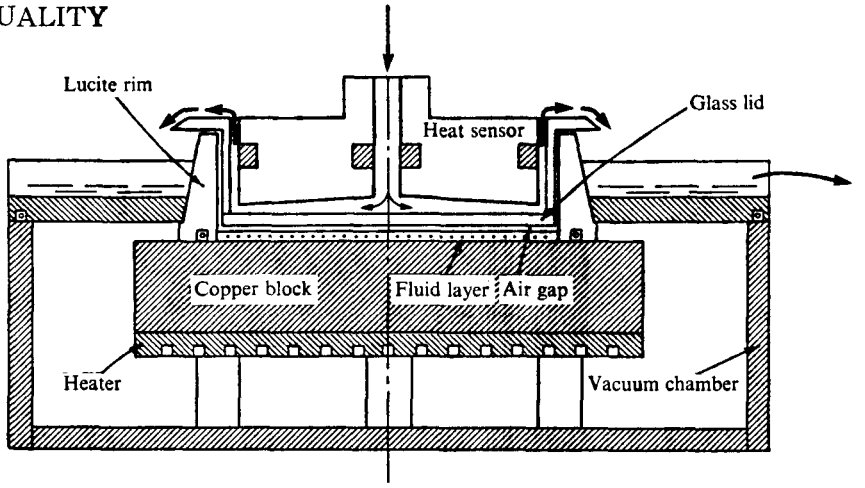

FIGURE 1. Schematic section though the convection apparatus.

by the onset of the convective motions. These two sets of experiments were made with fluid layers 2–5 mm deep. We will show in the following that one has to go to layers less than 2 mm deep in order to observe purely surface-tension-driven motions. Bénard's experiments were made with fluid layers of depths ranging from about 1 mm to about 0.5 mm.

2. Description of the apparatus

The apparatus used is a modified version of an apparatus used previously by Koschmieder & Pallas (1974*a*). A schematic diagram of the apparatus is shown in figure 1. The bottom of the fluid layer was a 5 cm thick copper block, which was heated from below by an electric current going through a resistance wire. The wire was cemented in circular grooves in a brass plate. The excellent thermal conductivity and the thickness of the copper block in combination with poor thermal conduction on top assure that the temperature at the top of the copper plate is practically uniform, as is required for comparison with the theories describing Bénard convection. To avoid lateral heat losses the copper block was placed in a vacuum tank. The copper plate was covered by shallow layers of silicone oil, bounded laterally by a circular lucite rim of 13.55 cm diameter. With a fluid depth of say 1 mm the aspect ratio of the fluid, defined as the ratio of the horizontal extension of the fluid divided by the fluid depth, was 135. The fluid was cooled from above through a very thin layer of air between 0.3 and 0.5 mm deep. The air was bounded on top by a glass plate 2.3 mm thick. The glass plate was the bottom of a lid in which water was circulated at a rate of 80 $cm^3\ s^{-1}$ in order to fix the temperature of the glass plate and thereby the temperature on top of the fluid.

Most of the space above the glass plate was filled usually with the so-called heat sensor, a device to measure the increase of the temperature of the cooling water caused by the heat transferred through the fluid layer and the air above it. The heat sensor is essentially a thermopile of 10 thermocouples in series, measuring the temperature difference between a copper ring surrounding the water inlet and copper ring being in contact with the cooling water after it passed over the glass plate.The heat sensor

has been described in detail elsewhere (Koschmieder & Pallas 1974*b*). Temperature differences of 0.001 °C between the incoming and outgoing water can be measured with the heat sensor. From the measured temperature increase of the cooling water follows the heat flux through the fluid layer, as will be discussed later.

The cooling water was taken from a 50 l insulated tank filled with water. The temperature of the water in the insulated tank was controlled by a heat exchanger whose temperature was determined by water coming from a commercial regulated water bath. Cooling water cannot be used from the water bath directly as the heat sensor is too sensitive. The heat sensor picks up the fairly regular fluctuations of the water temperature of the bath, which are caused by the heating and cooling of the temperature control. The enormous heat capacity of the water in the insulated tank reduces the fluctuations of the water-bath temperature. A steady signal for the temperature difference between incoming and outgoing water was then obtained.

3. The experiments

3.1. *Pattern formation*

The fluid motions were made visible by aluminum powder suspended in the fluid, which was either 100 cs silicone oil, or in some cases 50 cs silicone oil (Dow Corning 200 fluid). The properties of both fluids are listed in table 1. All experiments were made in a nearly steady state, it took usually about eight hours to heat up the fluid from rest at zero temperature difference to the highest temperature difference applied, which was in the maximal case about 60 °C between the copper plate and the glass lid. The fluid depth in the experiment shown in figure 2 was 1.37 mm, the depth of the air gap on top of the fluid was 0.5 mm.

When the fluid layer is heated up the first faint sign of motion is, besides a strong roll along the rim, a system of circular concentric rings, see figure 2(*a*). There are, in this picture, two stronger individual cells, which are caused by two impurities which have come into the fluid with the aluminum powder. The convecting fluid is seen on the shiny copper plate through the lid covering the fluid layer. The lid is filled with cooling water in order to maintain the temperature difference across the fluid. The heat sensor is taken out of the lid. Increasing the temperature difference causes the rings in figure 2(*a*) to break up into cells, figure 2(*b*). The cells clearly have a centre, the cell outline on the other hand is rather weak and not regular, certainly not of a regular hexagonal form. Increasing ΔT further intensifies the cells, figure 2(*c*). The cell boundaries then become outlined by floating aluminum powder which is extruded from the fluid. In figure 2 a larger than usual amount of aluminum powder was added to the fluid in order to be able to see the flow on photographs. In figure 2(*c*) the extruded aluminum powder can be seen floating on the surface of the fluid in the space between the outermost ring of cells and the clearly visible rim roll.

When the temperature difference is increased further a very definite change in appearance of the cells occurs spontaneously at a certain reproducible (critical) temperature difference ΔT_2, as can be recognized clearly in figure 2(*d*). The new type of cell is strikingly reminiscent of Bénard cells as we have seen them many times before, a good example of such a pattern can be found in Koschmieder (1974). As the hexagonal cells form, the floating aluminum powder, which outlined the cells of the first pattern, disappears from the surface of the fluid. Some aluminum powder then settles at the bottom in the centre of the cells underneath the uprising fluid. The settled powder can be recognized as little black specks in figure 2(*d*). The appearance of the hexagonal cells is also accompanied by an increase of the heat flux

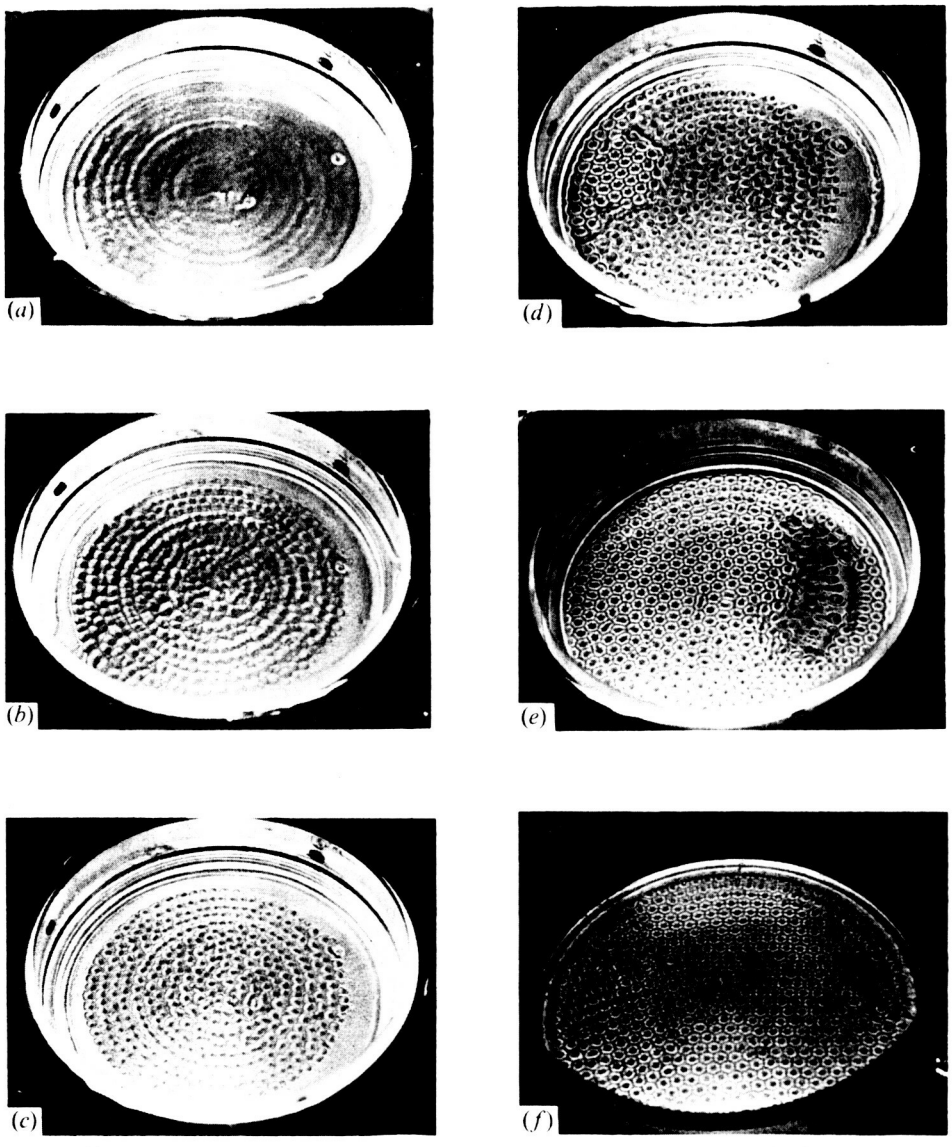

FIGURE 2. Visualization of the onset of convection in a layer of silicone oil of 100 cs viscosity, 1.37 mm deep, with an air gap of 0.51 mm. (*a*) $\Delta T = 0.57\ \Delta T_2$; (*b*) $0.72\ \Delta T_2$; (*c*) $0.86\ \Delta T_2$; (*d*) $0.95\ \Delta T_2$; (*e*) ΔT_2; (*f*) $1.08\ \Delta T_2$.

through the fluid layer, as will be shown later. A truly critical transition should, under ideal conditions, occur simultaneously over the entire area of the fluid. We have not observed such a genuine transition because of experimental difficulties. In particular, we cannot keep the depth of the air layer uniform over the entire area of the fluid layer. The reason for this is that the glass plate of the lid has to be glued to the frame of the lid. We have not been able to do this with an accuracy better than (at best) $\pm\frac{1}{100}$ mm. But $\frac{1}{100}$ mm is a substantial fraction of the gap between the fluid and the glass, which ranges from 0.3 to 0.5 mm in different experiments. A large portion, in many cases actually the larger part, of the applied temperature difference between

ν (cm²/s)	ρ (g/cm³)	α (°C^{-1})	κ (cm²/s)	S (dyne/cm)	dS/dT (dyne/cm °C)
1.00	0.968	0.000 96	0.001 095	19.36	−0.050
0.50	0.960	0.001 04	0.001 025	18.35	−0.047

TABLE 1. Properties of the fluids at 25 °C

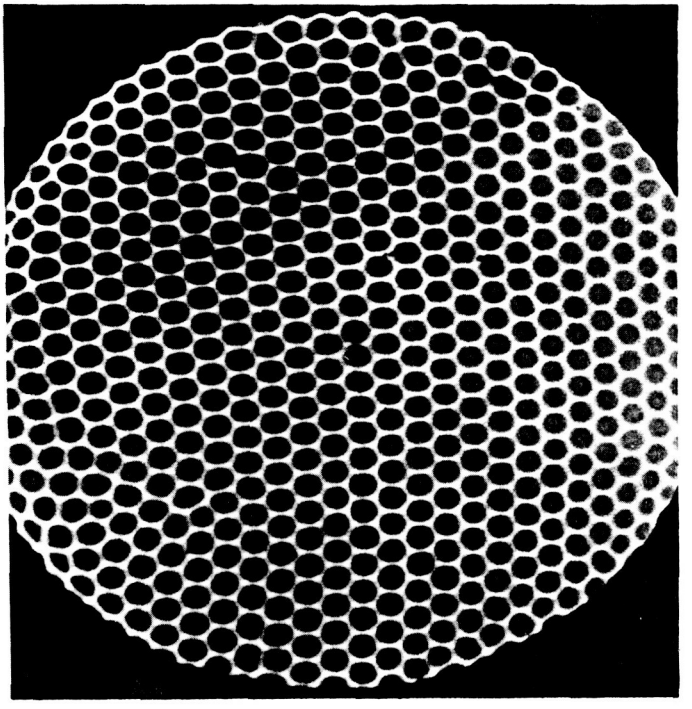

FIGURE 3. Shadowgraph of the hexagonal pattern at $\Delta T = 1.19\,\Delta T_2$. Viscosity 100 cs, fluid depth 1.35 mm.

the copper and the glass lid falls off in the air gap because of the very poor thermal conductivity of air. An air gap of unequal depth therefore causes a one-sided temperature distribution on top of the fluid. Hence the onset of the transition is one-sided.

When the temperature difference is increased further the hexagonal cells spread over an increasing area of the fluid, see figure 2 (*e*). Finally figure 2 (*f*) shows hexagonal cells covering the entire surface of the fluid. In this photograph the lid has been removed, so that one can see the rim of the layer with the rim roll, which was obscured in figure 2 (*a–e*). There are about 200 regular hexagonal cells in the pattern in figure 2 (*f*). When the slightly supercritical temperature difference is maintained another strange twist in the behaviour of the aluminum powder occurs. The small heaps of settled aluminum powder underneath the cell centres disappear, which means that the powder goes back into solution. This has never happened before in our experiments with deeper fluid layers. The peculiar behaviour of the aluminum powder does not seem to have fluid dynamics significance, but is an indication that surface forces play a role in the experiments with very shallow layers.

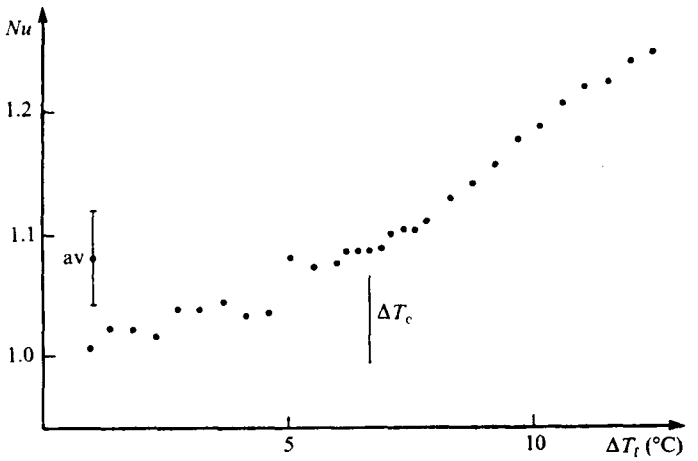

FIGURE 4. Heat transfer in the 1.81 mm deep fluid layer of 100 cs viscosity.

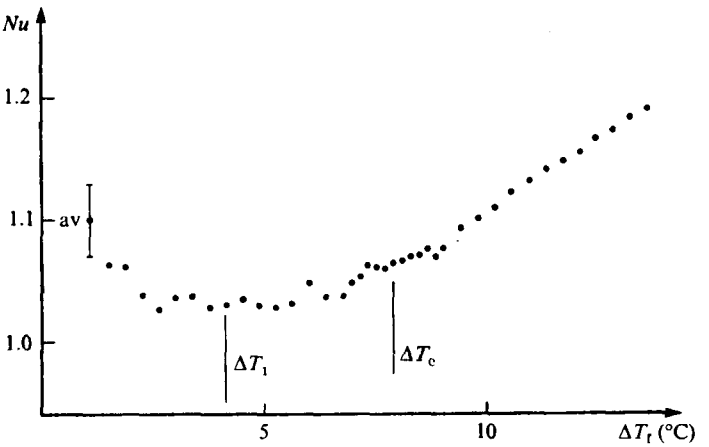

FIGURE 5. Heat transfer in the 1.31 mm deep fluid layer of 100 cs viscosity.

There is another way to visualize the fluid motions, namely the shadowgraph technique described by Silveston (1958). A parallel beam of white light is shone through the fluid layer where it is reflected from the bottom. The index of refraction in the fluid varies with temperature and consequently varies locally in the fluid with the temperature in the convective cells. The optical path of the light in the fluid layer is therefore different in different parts of a cell. Interference occurs therefore in the reflected light beam, outlining the cell pattern. We were not able to obtain a shadowgraph from the first pattern when the applied temperature difference was substantially below ΔT_2, regardless of whether we used the copper plate or a glass mirror placed on the copper plate as the bottom of the fluid. The surface of the copper block produces a shadowgraph of the second, hexagonal pattern, with minor imperfections resulting from the remaining uneveness of the copper surface caused by the machining. Shadowgraphs of the hexagonal cells obtained with the mirror were nearly perfect, see figure 3. One has to keep in mind that the mirror changes the thermal boundary condition at the bottom of the fluid, replacing the excellent

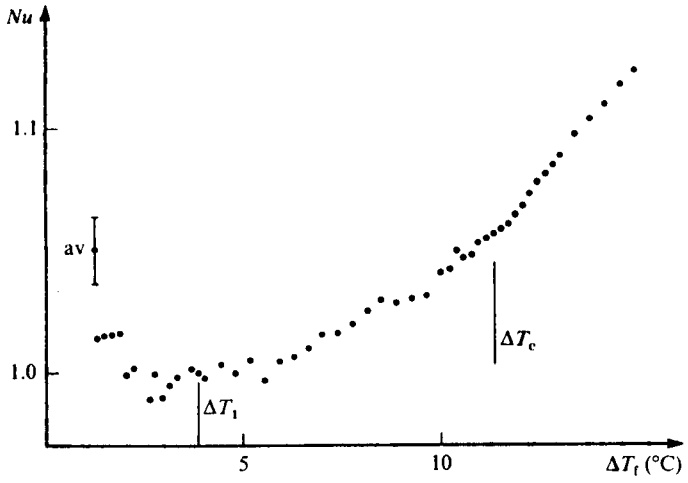

FIGURE 6. Heat transfer in the 0.93 mm deep fluid layer of 100 cs viscosity.

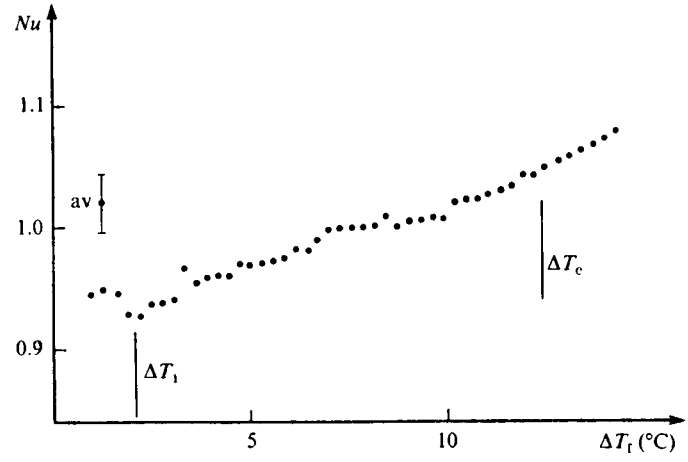

FIGURE 7. Heat transfer in the 0.72 mm deep fluid layer of 100 cs viscosity.

thermal conductivity of copper by the poor thermal conductivity of glass. The convective flow visualized by shadowgraphs with either the copper bottom or the mirror was nevertheless the same as the flow visualized with the aluminum powder.

3.2. *Heat flux measurements*

The usual procedure to determine the critical temperature gradient for the onset of convection is via the break of the heat transfer curve brought about by the additional heat transfer of the convective motions, a method introduced by Schmidt & Milverton (1935). The results of our heat transfer measurements are shown in figure 4–7. The heat flux when plotted in absolute units, or, for example, as microvolts measured by the heat sensor, has such a small change of slope with the onset of convection that the critical temperature difference cannot be determined accurately from the break of the curve. The heat flux in figures 4–7 is therefore plotted in units of the Nusselt number, which is the ratio of the actual heat flux divided by the heat flux caused

by the thermal conductivity of the fluid only. On a plot of Nusselt number versus applied temperature difference the break of the heat transfer curve is much more easily recognizable. The value of the Nusselt number before onset of convection is 1.

The abscissa in figures 4–7 is the temperature difference ΔT_f applied to the fluid. This temperature difference cannot be measured directly, because there is no space in the air gap above the fluid layer to mount thermocouples. The value of ΔT_f has to be calculated from the temperature difference ΔT between the copper plate and the cooling water. For the heat flux measurements we did not use the glass plate on top of the air layer, but a copper plate of 2 mm thickness. This was done to avoid additional corrections for the temperature drop in the glass. The value of ΔT_f is given by

$$\Delta T_f = \frac{\Delta T}{\left(1+\frac{\bar{\lambda}_f \Delta Z_a}{\bar{\lambda}_a \Delta Z_f}\right)}, \tag{1}$$

where $\bar{\lambda}_f$ is the mean thermal conductivity in the fluid layer, $\bar{\lambda}_a$ the mean thermal conductivity in the air layer, ΔZ_a the depth of the air layer and ΔZ_f the depth of the fluid layer. ΔT can be measured with an accuracy better than 1 %. Both thermal conductivities are known only with about 1 % accuracy. The depth of the fluid is known to about 1 %, while the depth of the air layer, which is of order 0.5 mm or less, is known at best with only 2 % accuracy. So the cumulative uncertainty in the value of ΔT_f is at least 5 %. Since the Nusselt number is proportional to ΔT_f, the experimental values of Nu can differ from 1 by ± 5 % or more. It is likely that the uncertainty in the value of Nu will increase with decreased ΔZ_a and ΔZ_f, because in particular the uncertainty in ΔZ_a becomes increasingly large. All measurements of Nu give the mean value of the heat flux at a given ΔT_f determined by four experiments. The standard deviation of the four measurements determines the experimental error of the heat flux measurement. Since so many error bars would confuse the graphs, only the average value of the error bars is indicated in the figures.

We will discuss the heat flux curve of the fluid layer with 1.81 mm depth (figure 4) first. In this case it appeared from corresponding visual observations that at $\Delta T_f \approx 6.6$ °C a hexagonal pattern had established without a prior first pattern. There is, of course, an uncertainty in the visual determination of ΔT_2, because the pattern does not form spontaneously over the entire fluid. This uncertainty is of the order of 5 % of ΔT_2. As can be seen in figure 4 the heat flux is, within the experimental error, about $Nu = 1.03$ for ΔT_f up to 5 °C, then it seems to increase prior to the observed $\Delta T_2 = 6.68$ °C, and increases steadily after ΔT_2. As we will see in the data evaluation it appears that with this fluid depth the formation of the first pattern has just taken place prior to the formation of the hexagonal cells. This is also indicated by the increase in the measured Nu before ΔT_2. The increase of Nu after ΔT_2 is in agreement with expectations.

With a fluid layer of 1.31 mm (figure 5) we observed visually the formation of the first pattern at $\Delta T_1 \approx 3.7$ °C. Our heat flux measurements indicate an increase of the Nusselt number for values of $\Delta T_f < 3.7$ °C. This is caused by an erroneous signal of the heat sensor. At very small values of ΔT_f the heat flux through the fluid layer is very small. The temperature increase in the coolant measured by the heat sensor is then determined mainly by heat generated by dissipation in the cooling fluid, as it moves from the inlet over the lid to the outlet. The contribution of dissipation to the heat sensor signal decreases as the heat flux to the lid from underneath increases.

In order to obtain a signal from the heat sensor which is less affected by dissipation in the coolant, we have, in all heat flux measurements, reduced the flow rate of the cooling water to 20 $cm^3\ s^{-1}$. For values of ΔT_f between ΔT_1 and ΔT_2 at ≈ 7.9 °C the heat flux in figure 5 increases on average just a little, then increases steadily and at a faster rate after ΔT_2. There is, of course, no abrupt change in the slope of the heat transfer curve at ΔT_2 because we are dealing here with the gradual transformation of a pattern, as shown in figure 2 (*d–e*).

Figure 6 shows the heat flux for a fluid layer of 0.93 mm depth, and figure 7 for a depth of 0.72 mm. It can be seen on these figures that the critical temperature difference ΔT_2 for the formation of the hexagonal cells increases with decreased depth, while on the other hand the temperature difference ΔT_1 for the formation of the first pattern decreases with decreased depth. The values of these temperature differences for the different fluid layers are listed later in table 2. It is already apparent in figure 6 and seems to be certain in figure 7 that the heat flux through the fluid layer is no longer constant after the formation of the first pattern, but increases with increased ΔT_f. This means that the motions in the cells of the first pattern are sufficiently fast to transfer an additional amount of heat. The formation of the hexagonal cells is still marked by a clear break in the heat flux curve in figure 6, at the temperature difference at which we visually observed the transition. In figure 7 however the break in the heat flux curve is barely recognizable. This probably means that near ΔT_2 the motions in the first pattern have become so vigorous that they hardly differ from the velocity of the flow in the hexagonal cells.

We have also measured the heat flux for two fluid layers of 50 cs silicone oil. Since there is no additional significant feature in these measurements their curves will not be shown.

3.3. *Data evaluation*

In order to understand the meaning of our observations the various experimental data have to be expressed in terms of the non-dimensional parameters involved. Buoyancy driven convection is governed by the Rayleigh number, which is

$$R = \frac{\alpha g \Delta T d^3}{\nu \kappa}, \tag{2}$$

with the volume expansion coefficient α, the acceleration of gravity g, the depth of the fluid d, the kinematic viscosity ν and the thermal diffusivity κ. The critical Rayleigh number R_c for onset of convection in a fluid layer with a free surface is $R_c = 1100.6$. This value of R_c applies when the top free surface is an excellent thermal conductor. Air on top of the fluid however approximates an insulating top boundary. The critical Rayleigh number in this case is then $R_c = 669$ (Nield 1964).

Surface-tension-driven convection is governed by the Marangoni number, which is

$$Ma = \frac{\mathrm{d}S}{\mathrm{d}T} \frac{\Delta T d}{\rho \nu \kappa}, \tag{3}$$

where $\mathrm{d}S/\mathrm{d}T$ is the variation of the surface-tension coefficient with temperature, d is again the depth of the fluid, and ρ is the density of the fluid. The critical Marangoni number Ma_c with an insulating top boundary is $Ma_c = 79.6$ (Nield 1964).

Table 2 gives, for different fluid depths, the values of the temperature difference for the appearance of the first pattern ΔT_1, the temperature difference for the appearance of the hexagonal cell pattern ΔT_2, and the corresponding Rayleigh and

No.	d (mm)	ΔT_1 (°C)	ΔT_2 (°C)	R_1	M_1	R_2	M_2
			(100 cs)				
1	2.57	—	5.98	—	—	91.5	76.8
2	1.81	6.68	6.68	35.9	61.0	35.9	61.0
3	1.31	4.12	7.92	8.21	26.4	16.4	52.9
4	0.93	3.86	11.3	2.73	17.5	8.73	56.2
5	0.72	2.09	12.4	0.67	7.17	4.49	48.2
			(50 cs)				
6	1.34	2.88	5.16	13.8	37.0	25.4	68.0
7	0.93	2.74	6.82	4.40	24.5	11.5	63.8

TABLE 2. Temperature difference and non-dimensional numbers of the pattern formation

Marangoni numbers. The lower part of table 2 gives the same parameters for the experiments with the 50 cs oil.

In agreement with our visual observations and with the heat transfer measurements (figure 4) we have set the temperature difference for the onset of the first pattern in the 1.81 mm deep layer equal to the temperature difference for the appearance of the hexagonal pattern. Actually, the first pattern forms, with this fluid depth, just before the hexagonal pattern, but within the experimental error the temperature differences for the formation of both patterns coincide. As can be seen in table 2, the temperature difference at which the first pattern forms decreases systematically with decreased fluid depth, while the temperature difference for the formation of the hexagonal pattern increases with decreased depth. In the 0.72 mm deep layer the Rayleigh number for onset of the first pattern is < 1, the Rayleigh number for onset of the hexagons is only 4.5. The Marangoni number for onset of the first pattern in the 0.72 mm deep layer is only 7, i.e. much smaller than the critical Marangoni number. On the other hand the Marangoni numbers for onset of the hexagonal pattern are near the theoretical critical Marangoni number.

The values of the Rayleigh number as well as the Marangoni number for the onset of both patterns in the 50 cs oil are in each case larger than the corresponding values for the 100 cs oil. The differences are too large to be explained by the experimental uncertainties. There are, on the other hand, not enough data to decide whether or not there is a systematic shift to higher non-dimensional numbers with the 50 cs oil. We emphasize that the visual observations with both oils gave completely analogous results.

We note that the uncertainty in the values of the Rayleigh numbers is of the order of 10%, because ΔT is known only to about $\pm 5\%$, as discussed before. The depth d is known to about 1%, so d^3 is known to about 3%, ν and κ are both known to 1%. The uncertainty in the values of the Marangoni numbers is also of the order of 10%. We have measured the value of $\mathrm{d}S/\mathrm{d}T$. The tensiometers used to determine S are accurate to only 1%. On the other hand, $\mathrm{d}S/\mathrm{d}T$ is quite small, so the error in the determination of $\mathrm{d}S/\mathrm{d}T$ is much larger. We have measured $\mathrm{d}S/\mathrm{d}T$ before (Koschmieder 1967) and found for the 100 cs silicone oil $\mathrm{d}S/\mathrm{d}T = 0.058$ dyne/cm °C. Our present value $\mathrm{d}S/\mathrm{d}T = 0.050$ dyne/cm °C is slightly smaller, but the difference is probably primarily the systematic uncertainty in determining $\mathrm{d}S/\mathrm{d}T$. We do not claim an

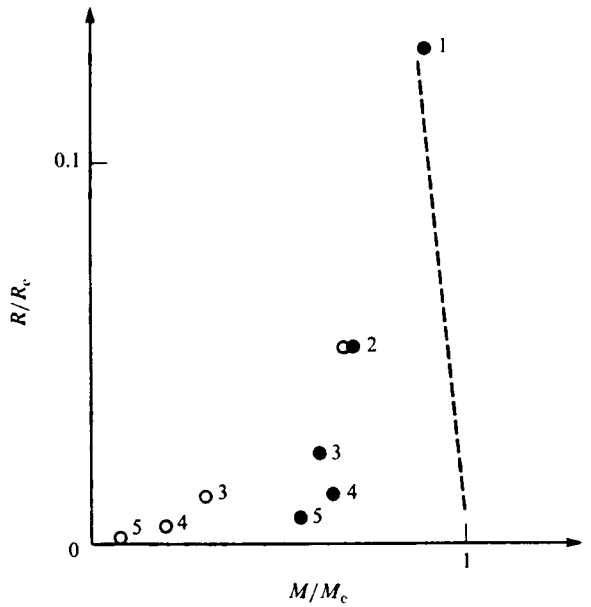

FIGURE 8. Comparison of the normalized Rayleigh and Marangoni number for the onset of convection of the two patterns. Open circles indicate first pattern, full circles indicate hexagonal pattern. The numbers refer to the different layers listed in table 2. The dashed line shows the expected onset of surface-tension-driven convection.

accuracy better than $\pm 5\%$. The uncertainty in the Marangoni number is of the order of 10%, because 5% comes from $\mathrm{d}S/\mathrm{d}T$, 1% each from ν and κ and 5% from ΔT.

For comparison with theory, in particular with figure 1 in Nield (1964), we divide the Rayleigh numbers and Marangoni numbers in table 2 by the corresponding critical numbers. However, the critical values of the numbers for the insulating free surface cannot be used now. The upper thermal boundary condition is taken into account by Nield via the parameter L, which is given here by $L = (\mathrm{d}Nu/\mathrm{d}T)\,\Delta T_f$. The values of $\mathrm{d}Nu/\mathrm{d}T$ follow from figures 4–7. The value of L for the five fluid layers listed in table 2 is $L = 0.19 \pm 0.02$. The critical Marangoni number with $L = 0.19$ is, according to Nield, $M_c = 86.8$, the critical Rayleigh number is then $R_c = 693.5$. Using these critical numbers we arrive at the points shown in figure 8. The dashed line in figure 8 shows the curve for the onset of convection in the presence of buoyancy and surface-tension effects. The critical curve can be written as $R/R_c + M/M_c \approx 1$. As we see in figure 8 the measured points for the onset of the hexagonal pattern are near the critical line. The points deviate from the expected value to lower values of M/M_c for the fluid layers with smaller depth. This seems to be a systematic effect. We speculate that this is caused by finite amplitude effects of the flow in the first pattern. Before the formation of the hexagons the motion in the first pattern seems to become so vigorous that the hexagons form prematurely, before one would expect the hexagons to form in a resting fluid layer. The vigorous motion in the first pattern is clearly documented by the increase of the convective heat transfer before the formation of the hexagons (figures 4–7).

The points in figure 8 which mark the onset of the first pattern are clearly subcritical from the point of view of the theory of convection caused by the surface-tension gradient $\mathrm{d}S/\mathrm{d}T$. As the thickness of the fluid layer increases the

difference in the Marangoni number of the onset of the two patterns decreases, until at around 2 mm depth (with this fluid) the hexagonal pattern becomes the only pattern to appear at all. On the other hand, the tendency of the first pattern to appear at ever smaller temperature gradients, or Rayleigh and Marangoni numbers, is quite obvious.

4. Discussion

The principal result of these experiments is the discovery of the unexpected first pattern. In order to observe this pattern it is necessary to work with fluid layers of small depth, in our case smaller than 2 mm. Small depth was involved in Bénard's observation that his cells formed at extraordinarily small Rayleigh numbers and is also a requirement for surface-tension forces to have their full impact.

It has been suggested that there may be three reasons for the theoretically unexpected formation of the first pattern, namely

(*a*) an experimental imperfection;

(*b*) a subcritical instability;

(*c*) an instability not contained in the conventional theories.

An experimental imperfection would be a deviation of the experimental set-up from the case studied in conventional theories, that is from the case of a plane motionless fluid on an infinite horizontal plate heated uniformly from below and cooled uniformly from above through the upper surface which is subject to surface tension effects.

In our apparatus such an imperfection is the meniscus of the fluid layer at the wall, which is not considered in the theories. The meniscus is a natural phenomenon occurring whenever a fluid layer is in a container. In reality the meniscus seems to pose more of a problem than one would expect. We have observed that the silicone oil moves up along the rim as a thin film to a height of over 1 cm if the applied temperature difference is large, probably a consequence of the vertical temperature gradient in the rim. However, the meniscus cannot be the cause of the first pattern because one can arrange a fluid layer without a meniscus and still observe the first pattern. The meniscus was eliminated by containing the fluid with a thin lucite ring (of 102 mm diameter and about 1.4 mm depth). Fluid was put into the bowl formed by the copper bottom plate and the lucite ring so that the level of the fluid was plane with the top of the ring. The first pattern formed as usual.

In connection with the first occurrence of circular cells in our experiments it has been suggested that the first pattern may be caused by lateral heat loss or other radial temperature gradients, such as those caused by the misalignment of the top glass plate or by the non-uniformity of the temperature of the top glass plate caused by the temperature increase of the cooling water. Lateral heat loss in our experiments has practically been eliminated by surrounding the rim of the fluid with vacuum as indicated in figure 1. But this arrangement makes the vertical temperature gradient in the rim smaller than the temperature gradient in the fluid because the cooling at the rim is applied at a greater height above the copper plate than for the glass plate over the fluid layer (figure 1). At the level of the fluid the rim will be warmer than the fluid, i.e. there is a horizontal temperature gradient. However, the lucite rim is a very poor thermal conductor, while the copper on the bottom of the very thin silicone-oil layer is an excellent conductor. Even from the top of the fluid layer the uniform temperature of the copper plate is only about 1 mm away, while the rim is, for a large part of the fluid, some centimetres away. Furthermore, the thermal

conductivity of copper is about 2500 times better than the thermal conductivity of silicone oil. Thus it would require very large temperature differences between the rim and the fluid in order to create an effective horizontal temperature gradient in the interior of the fluid. Also, there is no mechanism known by which small-scale cells would be created via a horizontal temperature gradient in a fluid. Finally the experiment with the fluid contained by a small lucite ring does not support the concept of the significance of the lateral temperature gradient either, because in that set-up the fluid layer is separated from the rim of the apparatus by an air gap of 12 mm width. Air is an excellent thermal insulator which should shield the fluid effectively from the temperature distribution in the rim.

To investigate the non-uniformity of the temperature of the glass lid caused by the increase of the temperature of the cooling water, we measure this temperature increase with the heat sensor. For the extreme case of the lowest fluid depth (0.73 mm) and the largest applied temperature difference across the oil, the temperature increase of the cooling water amounted to 3% of the temperature difference across the oil. However, the temperature difference in the cooling fluid extends from the centre of the lid to the rim of the lid. If one compares the temperature gradients then the ratio of the temperature gradient across the lid to the vertical temperature gradient across the convecting fluid is about 2×10^{-4}. In order to see whether this has a noticeable effect on the formation of the pattern, we increased the flow rate of the cooling water from the 20 $cm^3\ s^{-1}$ used when we measured with the heat sensor, to the maximal flow rate with this pump which was about 80 $cm^3\ s^{-1}$. The ratio of the radial to the vertical temperature gradient was then 5×10^{-5}. No noticeable consequence of the increased flow rate was observed. We do not, therefore, believe that the radial temperature gradient in the glass lid is significant for the formation of the first pattern.

The misalignment of the plane of the glass lid with respect to the plane of the fluid surface discussed in §3.1 has a potentially greater influence on the uniformity of the top temperature of the fluid, than the non-uniformity of the temperature caused by the cooling. The consequences of the misalignment of the lid on the onset of the hexagonal pattern were obvious in all experiments, see e.g. figure 2(*d*). All efforts to improve on this situation had little or no success. Misalignment of the lid seemed to have little if any effect on the formation of the first pattern, which in all experiments, seemed to form essentially in an axisymmetric and not one-sided way. Figure 2(*a*, *d*) are from the same experiment and show that there is no apparent relation between the symmetry of the formation of the first pattern and the asymmetry of the formation of the hexagonal pattern.

Motion of the air between the fluid and the glass lid might also be the cause for the formation of the first pattern. However, the Rayleigh numbers of the air layer are, even with the highest temperatures applied, smaller than $10^{-3}\ R_c$. The prime reason for this is the very small depth of the air layer (≈ 0.5 mm) and the dependence of the Rayleigh number on the third power of the depth. It seems to be most unlikely that the first pattern is induced by motion of the air layer.

Finally, another possible experimental imperfection might be that the aluminum powder added to the fluid causes the formation of the first pattern. The aluminum powder settles gradually and causes a compensating upward motion of the fluid. However, one would expect any possible effect of the settling of the powder to be smaller in the shallow layers of fluid than in deep layers, because the aluminum powder will settle sooner in the shallow layers and so it seems to be unlikely that the first pattern would appear preferentially in shallow fluid layers. One should also

expect an effect of the concentration of the aluminum particles. The concentration of the particles was varied substantially (we estimate by a factor of at least 10), mainly because of our efforts to take photographs of the flow which requires substantially bigger concentrations of the aluminum powder, but we did not notice any indication that this had influenced the appearance of the first pattern. We know of no theory that would predict the formation of a cellular pattern on the basis of the settling motion of an impurity in a fluid. Such a settling motion is not related to the diffusive two-component Bénard convection problem which has been reviewed by Schechter, Velarde & Platten (1974).

To summarize, we do not see a convincing reason for believing that the first pattern is caused by an imperfection of the experimental set-up.

Concerning the question of the possibility of a subcritical instability we note that a subcritical instability was predicted by Davis (1969). Later, Davis & Homsy (1980) and Castillo & Velarde (1982) elaborated on this topic. Of importance in connection with this problem is the value of the crispation number C, which is a characteristic parameter for the importance of the surface tension coefficient S. C is defined as $C = \mu\kappa/Sd$, where μ is the dynamic viscosity of the fluid. In our experiments the value of C is about 5.5×10^{-4}, so the deformability of the surface is very small. This means that the basic results concerning the subcritical instability are contained in Davis' (1969) paper. From figure 1 therein, it follows for $L = 0$ (we have $L = 0.2$) that the subcritical instability ranges from $Ma = 57$ to $Ma = 80$ at $R = 0$. However, in our experiments with the 0.72 mm deep layer the first pattern appears according to table 2 at $Ma = 7.2$ (with $R = 0.7$), which is deep in the stable region of figure 1 of Davis. So, although according to the energy method a range of instability is predicted which is at a lower Marangoni number than the critical value of the instability predicted by linear theory, the instability apparent in the first pattern that we observe is deep in the stable region according to the energy method. There is also the problem that the subcritical instability is probably associated with the appearance of the hexagonal pattern, and not a pattern of a different form as we observed.

An explanation of the first pattern can be sought in Scriven & Sternling's (1964) paper. The onset of convection driven by surface tension at ever smaller temperature gradients is actually predicted there. There are, however, difficulties. Scriven & Sternling predict that the small onset temperature gradients are accompanied by increased wavelengths or cell sizes. However, we did not observe in any of our experiments a noticeable difference in the size of the cells of the first pattern and the hexagonal pattern. The wavelength of the hexagonal pattern is determined by Nield's theory and does not change with decreased depth of the fluid. It can be seen in figure 2(*d*) that there is no significant difference in the cell sizes of the first pattern and the hexagonal pattern. We did not make a systematic survey of the cell sizes, but we believe that within $\pm 10\%$ accuracy the wavelength of the first pattern and the hexagonal pattern are the same. So there seems to be a discrepancy between the experimental observation and this aspect of Scriven & Sternling's results. Also, it follows from Smith (1966) and Davis & Homsy (1980) that only very small shifts in the critical Marangoni number are expected if the crispation number is as small as it is in our experiments.

Our experimental results for the onset of the hexagonal pattern, are in quite good agreement with the basic results of Pearson (1958) and Nield (1964). Nield's study seems to be particularly relevant because it incorporates gravity, which is present in the laboratory and is of such magnitude that it cannot easily be neglected. The fact that the hexagonal pattern appears in thin layers at subcritical Marangoni

numbers seems to be understandable as a finite-amplitude effect of the first pattern. It appears that Pearson's and Nield's theories correctly predict the consequences of the presence of the surface tension gradient $\mathrm{d}S/\mathrm{d}T$ on convective motions. So the formation of the first pattern, which appears neither in Pearson's nor in Nield's study, is not caused by the variation of surface tension with temperature.

Help and comments from Professor R. S. Schechter and Professor S. H. Davis are gratefully acknowledged. Mr S. Prahl has helped with the visualization experiments. Mr J. Gardner has measured the surface-tension coefficients. Support of this work through the National Aeronautics and Space Agency and through the National Science Foundation is also gratefully acknowledged.

REFERENCES

BÉNARD, H. 1900 *Rev. Gen. Sci. Pure Appl.* **1**, 1261–1271, 1309–1328.
BÉNARD, H. 1930 *Proc. 3rd. Int. Congr. Appl. Mech.* **1**, 120.
BLOCK, M. J. 1956 *Nature* **178**, 650–651.
CASTILLO, J. L. & VELARDE, M. G. 1982 *J. Fluid Mech.* **125**, 463–474.
CLOOT, A. & LEBON, G. 1984 *J. Fluid Mech.* **145**, 447–469.
DAVIS, S. H. 1969 *J. Fluid Mech.* **39**, 347–359.
DAVIS, S. H. & HOMSY, G. M. 1980 *J. Fluid Mech.* **98**, 527–553.
KOSCHMIEDER, E. L. 1967 *J. Fluid Mech.* **30**, 9–15.
KOSCHMIEDER, E. L. 1974 *Adv. Chem. Phys.* **26**, 177–212.
KOSCHMIEDER, E. L. & PALLAS, S. G. 1974*a* *Intl J. Heat Mass Transfer* **17**, 991–1002.
KOSCHMIEDER, E. L. & PALLAS, S. G. 1974*b* *Rev. Sci. Instrum.* **45**, 1164–1165.
KRASKA, J. R. & SANI, R. L. 1979 *Intl J. Heat Mass Transfer* **22**, 535–546.
NIELD, D. A. 1964 *J. Fluid Mech.* **19**, 341–352.
PALMER, H. J. & BERG, J. C. 1971 *J. Fluid Mech.* **97**, 779–787.
PEARSON, J. R. 1958 *J. Fluid Mech.* **4**, 489–500.
RAYLEIGH, LORD 1916 *Phil. Mag.* **32**, 529–546.
ROSENBLAT, S., DAVIS, S. H. & HOMSY, G. M. 1982*a* *J. Fluid Mech.* **120**, 91–122.
ROSENBLAT, S., HOMSY, G. M. & DAVIS, S. H. 1982*b* *J. Fluid Mech.* **120**, 123–138.
SCANLON, J. W. & SEGEL, L. A. 1967 *J. Fluid Mech.* **30**, 149–162.
SCHECHTER, R. S., VELARDE, M. G. & PLATTEN, J. K. 1974 *Adv. Chem. Phys.* **26**, 265–301.
SCHMIDT, R. J. & MILVERTON, S. W. 1935 *Proc. R. Soc.* A **152**, 586–594.
SCRIVEN, L. E. & STERNLING, C. V. 1964 *J. Fluid Mech.* **19**, 321–340.
SILVESTON, P. L. 1958 *Forsch. Ing. Wes.* **24**, 29–32, 59–69.
SMITH, K. A. 1966 *J. Fluid Mech.* **24**, 401–414.

Onset of Rayleigh-Benard Convection in Thin Fluid Layers

E. L. Koschmieder and J. R. Campbell

College of Engineering and I. Prigogine Center
for Statistical Mechanics
The University of Texas, Austin, Texas 78712, U.S.A.

The onset of Rayleigh-Benard convection in thin fluid layers heated uniformly from below has been studied experimentally. Subcritical motions have been found to occur if the depth of the fluid was smaller than 2 mm. The thinner the fluid layer was, the larger was the range in subcritical temperature differences over which the subcritical motions could be observed. Large temperature gradients are required to reach the critical temperature difference in the thin fluid layers. The variation of viscosity with temperature then make the fluid layer non-Boussinesq. The onset of convection in non-Boussinesq layers was found to take place in the form of hexagonal cells which transform at slightly supercritical temperature gradients into rolls, in agreement with theoretical predictions. Onset of Rayleigh-Benard convection under non-Boussinesq conditions was found to occur at Rayleigh numbers larger than the conventional critical Rayleigh number $R_c = 1708$.

1. Introduction

In an earlier investigation of convection in thin fluid layers under an air surface (Koschmieder and Biggerstaff, 1986) subcritical convective motions appeared prior to the formation of a hexagonal cell pattern at the critical Marangoni number, if the depth of the fluid

layer was less than 2 mm. This observation posed the question for the cause of these subcritical motions. This is an important question because it is one of the elementary tenets of the theory of hydrodynamic stability that the fluid remains completely at rest before the critical condition for onset of convection is reached. Experiments with convection under an air surface introduce a number of difficulties and uncertainties about the conditions and surface tension gradients at the fluid surface. It might have been one of those difficulties which caused the premature motions in the fluid. However, these uncertainties can be eliminated by putting a lid into contact with the fluid, thereby changing the experiment from a surface tension driven Benard convection experiment to a Rayleigh-Benard convection experiment in which the driving force is not surface tension gradients but buoyancy. We will see that, contrary to expectations, subcritical convective motions appear also in Rayleigh-Benard convection, provided that the fluid layer is sufficiently thin.

Working with thin fluid layers in Rayleigh-Benard convection requires large vertical temperature gradients since the critical temperature gradient is inversely proportional to the third power of the depth of the fluid. Large temperature gradients tend to make the problem non-Boussinesq, because of the variation of the viscosity of the fluid with temperature. The consequences of the variation of viscosity with temperature on the onset of Rayleigh-Benard convection have been studied in a number of papers, beginning with Palm (1960). Palm predicted the formation of a hexagonal pattern at a temperature difference smaller than the critical temperature difference of the Boussinesq case. The theoretical work on the consequences of the

variation of viscosity with temperature was continued by Stuart and Segel (1962), Palm, Ellingsen and Gjevik (1967), Busse (1967) and Davis and Segel (1968). These studies revealed that convection in variable viscosity fluids should start at subcritical values of the Rayleigh number with a hexagonal pattern which should, however, change to a roll pattern at slightly supercritical Rayleigh numbers. Part of this prediction has been confirmed experimentally by Hoard, Robertson and Acrivos (1970). They showed, that in a fluid in which the viscosity varied by a factor of about 10 between the top and bottom boundaries, the pattern of the flow at onset of convection was hexagonal and appeared at a temperature gradient smaller than the critical temperature gradient for the Boussinesq case. However, no subsequent transformation of the hexagonal pattern to a roll pattern was observed. All of the above mentioned studies were concerned with a small perturbation of the Boussinesq approximation by the temperature dependence of viscosity.

The onset of convection under highly non-Boussinesq conditions with very large variations of the viscosity has been studied by Stengel, Oliver and Booker (1982), and Oliver and Booker (1983). Using glycerol in their study the viscosity on top of the fluid layer differs by a factor of up to 3000 from the viscosity of the fluid at the bottom of the layer. Stengel et al. predicted that in the highly non-Boussinesq case the Rayleigh number for onset of convection is larger than the critical Rayleigh number in the Boussinesq case. The experiments described in Stengel et al. seem to confirm the increase of the critical Rayleigh number with increased viscosity ratio, although there are substantial experimental uncertainties in their

data, because the critical Rayleigh numbers are not determined from Nusselt number measurements. The flow pattern in such experiments is described in Oliver and Booker (1983). There are rolls if the viscosity variation is small, and hexagons with large viscosity variation. The hexagons change to square cells at higher supercritical Rayleigh numbers.

In the following we will describe experiments studying the onset of convection in a conventional fluid (silicone oil), in which the viscosity variation is comparatively small. The viscosity variation and its consequences are only a secondary topic which appears in our experiments as a necessary consequence of the prime objective, which is the study of the onset of convection in thin fluid layers.

2. The Apparatus

The apparatus was the same apparatus that was used in Koschmieder and Biggerstaff (1986), where a sketch of the equipment is shown. In all experiments described in the present paper the lid was in contact with the fluid layer. We can list here only the most elementary features. The bottom of the fluid layer is a 5 cm thick circular copper block, heated electrically from below. The lateral confinement of the fluid is a lucite ring of 13.55 cm inner diameter. The fluid layer was cooled from above by water from a constant temperature bath. The water flowed either over a sapphire crystal for the visualization experiments or over a copper plate for the heat flux measurements. The sapphire is the same as the one used in the experiment of Koschmieder and Pallas (1974a), where such a sapphire was used for the first time in a convection experiment. The advantage of the sapphire is its good thermal conductivity in spite of its transparency. The

sapphire makes it possible to visualize the entire fluid layer and yet to realize closely the (perfect) thermal conduction condition assumed in theory at the horizontal boundaries. The sapphire has a diameter of 13.335 cm and a thickness of 0.508 cm, its top and bottom surfaces are polished.

The lid, either the sapphire or the copper plate, were supported from below by lucite rings of various thickness, all with an inner diameter of 12.38 cm. Since the fluid must be provided with space to expand when the fluid is warmed up, the lucite rings were separated from the lid by three spacers 0.0025 cm thick. So the fluid had at its outside around the circumference a gap of 0.0025 cm depth into which the fluid could expand. The axisymmetry of the setup was preserved in this way. For the heat flux experiments the space on top of the lid was filled with the heat sensor, a device to measure the increase of the temperature of the cooling water as it passed over the lid covering the heated silicone oil layer. From the temperature increase of the cooling water follows the heat flux through the silicone oil. The heat sensor is described in detail in Koschmieder and Pallas (1974b).

Flow visualization was accomplished by the shadowgraph technique, introduced by Silveston (1958). A beam of white light is shone from above through the oil layer, reflected on the bottom of the layer and experiences interferences on a screen a distance behind the apparatus. The interferences are caused by the different path length of the light in the fluid, which vary because of the variation of the index of refraction with temperature. The interference pattern correspond to the horizontal variation of the temperature field in the fluid, which is

caused by the pattern of motion in the fluid. The interpretation of shadowgraph patterns has recently been discussed by Jenkins (1987). For the shadowgraph technique to work, one needs a reflecting bottom of the fluid. The copper block has a near mirror finish, but is not good enough to serve as a mirror for a shadowgraph. We have therefore placed either a chrome plated stainless steel mirror of 0.8 mm thickness or a glass mirror of 3.2 mm thickness on the bottom of the fluid in the visualization experiments. It would have been too expensive to buy a metal mirror of this size with an optical surface.

3. The Experiments

3.1 Pattern Formation

It is necessary to verify the correct functioning of the apparatus under conventional conditions before we go on to study the existence of subcritical motions in Rayleigh-Benard convection. In order to prove that the apparatus works properly we have studied the onset of convection in a 5 mm deep layer of silicone oil of 1 cm^2/sec viscosity. The conditions are then not strictly Boussinesq, the critical temperature difference being 14.5°C and the viscosity ratio ν_{max}/ν_{min} = 1.15. But we have observed before (Koschmieder, 1965) that under these conditions a pattern of circular concentric rolls formed in a circular container, just as the same pattern formed in a 1 cm deep layer of the same oil, when the critical temperature difference was only 2°C and the conditions were certainly Boussinesq .

In the experiment with the 5 mm deep layer the fluid was heated for 4 hours to the critical theoretical temperature difference ΔT_c = 14.5°C. At that temperature difference a weak pattern appeared on the shadowgraph, on which prior to that ΔT no pattern was visible at all.

The pattern at ΔT_c consisted of circular concentric rolls with some weak cellular divisions. Thirty minutes later, at a temperature difference of 16.0°C or 1.10 ΔT_c an intense pattern of regular circular concentric rolls had formed, as is shown in Fig. 1a. We have observed such circular pattern before in Koschmieder (1965) and Koschmieder and Pallas (1974a). It is worth noting that the configuration of the circular lateral confinement of the fluid was different in the case here as well as in the two other cases, the differences of the wall configurations being necessitated by the particular purpose of each of these experiments. Nevertheless, we have observed perfect axisymmetric patterns in each of these experiments. The bright circles in Fig. 1a indicate the location of descending fluid motions. There is one additional bright ring just outside of the field of view of the photograph. There are therefore 12 circular concentric rolls in the fluid layer in agreement with the aspect ratio of the layer, which is $\Gamma = 2r/d = 24.7$. When the temperature difference across the fluid was slowly increased to higher supercritical values, the diameter of the center roll shrunk (Fig. 1b), the width of the bright rings increased, and wall effects in the form of rolls oriented perpendicular to the wall became apparent. Ten hours after the experiment had started and at $\Delta T = 2.33\ \Delta T_c$ the center roll had been reduced to a very bright spot (Fig. 1c), indicating the increase of the wavelength of the convective motions with increased supercritical Rayleigh-number, which we had first noted in Koschmieder (1965). Having confirmed the essential features of Rayleigh-Benard convection in the Boussinesq case in this apparatus, we could proceed to experiments with non-Boussinesq conditions.

With a fluid layer of 4 mm depth and the silicone oil of 1 cm^2/sec viscosity the onset of convection is expected at $\Delta T = 25.0°C$. The viscosity ratio is then $\nu_{max}/\nu_{min} = 1.29$, meaning that the conditions are no longer Boussinesq. Onset of convection in the experiment occurred at $\Delta T = 26.25°C$ in the form of a circular pattern with a superposed cellular structure, see Fig. 2a. Prior to this ΔT no pattern was visible on the shadowgraph. Increasing the temperature difference by 1°C to $\Delta T = 1.05\ \Delta T_c$ eliminated the cellular structure completely (Fig. 2b). The events were qualitatively the same as with the 5 mm deep layer only that the cellular pattern at onset of convection was much more conspicuous and a little more persistent. In Fig. 2b there are more bright rings than in Fig. 1a because the aspect ratio of the fluid layer is different, being $\Gamma = 30.95$ with the 4 mm deep layer. There is then space for 15 concentric rolls with sinking motion in the center of the layer. The sinking motion there appears as the bright center point in Fig. 2b. The rays which go out to the right and left from the fluid in the photograph Fig. 2b originate from an optical distortion caused by the lucite wall of the lid. The sequence of events shown in Fig. 2a, 2b is in qualitative agreement with the theoretical prediction that in a slightly non-Boussinesq fluid the onset of convection occurs in the form of hexagonal cells which transform to a roll pattern if the temperature gradient is increased slightly. The occurrence of this transformation has, to our knowledge, not been shown before. We will discuss the quantitative aspects of this problem when we come to the heat flux measurements.

The experiments of Koschmieder and Biggerstaff (1986) showed that subcritical motions in surface tension driven convection appear only

if the layer is sufficiently thin, and that the range of subcritical flow increases with decreased depth of the fluid. We looked therefore for the appearance of subcritical flow in Rayleigh-Benard convection in fluid layers of about 2 mm depth or less. It is then necessary to use oil of 0.10 cm^2/sec viscosity, because with the 1 cm^2/sec silicone oil the critical temperature difference would be about 200°C, which is impractical. With a 2.10 mm deep layer, the 0.10 cm^2/sec silicone oil, a glass mirror at the bottom, and the sapphire lid, a weak subcritical pattern of ill defined small scale rolls appeared on the shadowgraph at a temperature difference of 15°C. When the temperature difference was increased the pattern became a little more intense, and transformed at 18.75°C rapidly into a very intense cellular pattern. This marked the critical condition. We will show later that the appearance of the strong cellular pattern coincides with the break in the heat flux curve, which has traditionally been considered the proof for onset of convection. Since the range of subcritical flow is small, the results of this experiment may be inconclusive and we will proceed to the experiments with the smallest fluid depth tried.

First, however, we add a comment concerning the use of the glass mirror in these experiments. The glass mirror is undesirable because of the thickness of the glass (3.2 mm) and its comparatively poor thermal conductivity whose accurate value we do not know. The glass mirror has, however, the advantage of a far more uniform reflectivity than the chrome plated steel mirror. Looking at a shadowgraph of a fluid layer at rest above the steel mirror one sees a grainy (black and white) texture; while the glass mirror under the same conditions shows a uniform bright image. The texture on the image of the steel

mirror makes the steel mirror unsuited for the observation of subcritical motions whose shadowgraph image is so weak that it cannot be distinguished from the texture of the steel mirror. If, on the other hand, the flow is critical or supercritical, then the interference pattern of the shadowgraph is so strong that the texture of the mirror cannot be seen anymore, as is, for example, the case in Figs. 1a-c and 2a-b. We have, however, made certain that the subcritical motions to be discussed in the following are not a consequence of the glass mirror. One can indeed see subcritical motion on the steel mirror, but its pattern is superposed on the image of the texture of the mirror, and this combination of two images is useless for the determination of the form of the subcritical flow. Pictures of the shadowgraph of subcritical flow can be taken only after all cooling fluid on top of the sapphire has been removed, because even a few millimeters of water on top of the lid wash out the interference of the light beam. It takes about half a minute to remove the heat sensor on top of the sapphire as well as all the cooling fluid, take a photograph and putting the heat sensor back in place. If the fluid underneath the lid is critical or supercritical water on top of the lid does not interfere with the shadowgraph, although fringe effects, such as the rays on Fig. 2b, increase.

With a fluid depth of 1.63 mm, the 0.10 cm^2/sec silicone oil, the glass mirror on the bottom of the fluid, and the sapphire lid, subcritical flow appeared at a temperature difference of 17.5°C = 0.45 ΔT_c. The flow was in the form of a very weak pattern of small-scale rolls. The shadowgraph was so weak that a photograph could not be taken. We note that the subcritical motion appeared at a much lower

value of $\Delta T/\Delta T_c$ than the value at which they had appeared with the 2.10 mm deep layer ($\Delta T/\Delta T_c = 0.8$). This is analogous to our observations with surface tension driven convection (Koschmieder and Biggerstaff, 1986). We also note that the appearance of the subcritical flow does not seem to be a critical phenomenon. With increased ΔT subcritical flow apparently develops continuously from an imperceptible to a barely perceptible flow.

Increasing the temperature difference across the fluid increased the intensity of the shadowgraph a little. At $\Delta T = 28.75°C = 0.74\ \Delta T_c$ the first photograph was taken (Fig. 3a). One sees very weak, somewhat irregular short rolls which cover the entire plate. Increasing the temperature difference further intensified the subcritical motions only slightly, at $\Delta T = 32.5°C = 0.84\ \Delta T_c$ the flow looked like Fig. 3b. The pattern had changed very little as compared with Fig. 3a. At $\Delta T = 35.0°C = 0.90\ \Delta T_c$ the pattern (Fig. 3c) had a much more cellular structure than before, but was still subcritical. At $\Delta T = 38.75°C\ \Delta T_c$ a very strong intensification of the image of the shadowgraph occurred, see Fig. 3d. The pattern consisted then of a very large number of hexagonal cells with one small patch of forming rolls. This pattern marked the critical condition. The temperature difference $\Delta T = 38.75°C$ is the temperature difference between the copper block and the cooling fluid on top of the sapphire. The temperature drop on the glass plate is therefore included in the value of ΔT. The heat flux measurements show that the critical temperature difference with copper-copper boundaries of the fluid is actually 30.8°C. The viscosity variation of the fluid at this temperature difference is $\nu_{max}/\nu_{min} = 1.68$, so the conditions are non-Boussinesq.

Onset of convection in the form of hexagonal cells fits the theoretical description of the consequences of weak non-Boussinesq conditions, as well as our observations with the 4 mm deep fluid layer.

Increasing the temperature difference across the fluid to supercritical values brought about a rapid transformation of the hexagonal cell pattern to a pattern of rolls. At $\Delta T = 40°C = 1.03\ \Delta T_c$ the patch of forming rolls had become unquestionable rolls (Fig. 3e), and at $\Delta T = 42.5°C = 1.1\ \Delta T_c$ (Fig. 3f) the rolls had spread over most of the layer. Out of concern for the sapphire the temperature difference was then not increased further. The quite obvious transformation of the hexagonal cells to rolls is again in agreement with theoretical expectations for the weakly non-Boussinesq case. The non-Boussinesq effects are now so strong as to overcome the, by design, weak effects of the lateral wall. So in spite of being contained by a circular boundary the pattern in Fig. 3f is not circular and concentric as it was in Fig. 1 and Fig. 2.

The prime result of this experiment is the observation of the existence of subcritical flow in Rayleigh-Benard convection over a large range of subcritical Rayleigh numbers. As a by-product of this experiment we have learned again that the onset of Rayleigh-Benard convection in a non-Boussinesq fluid layer takes place in the form of a pattern of hexagonal cells which change into rolls at slightly supercritical Rayleigh numbers.

3.2 Heat Flux Measurements

Since the experiments of Schmidt and Milverton (1935) heat transfer measurements have frequently been used in order to determine quan-

titatively the onset of convection. The onset of convection follows from the so-called "break" in the heat transfer curve. The break of the heat transfer curves occurs at that ΔT at which thermal conduction through the fluid layer by the molecular conductivity of the fluid is supplemented by heat transferred through the motion of the fluid after onset of convection. The heat transfer curves are usually plotted using the Nusselt number Nu as ordinate. The Nusselt number is the ratio of the actual heat flux to the heat flux caused by thermal conduction only, in a formula

$$Nu = \frac{Qconv + Qcond}{Qcond} \qquad (1)$$

Before onset of convection we have Nu = 1 for all values of the temperature difference applied to the fluid layer. In the experiments described in the following the value of the Nusselt number was determined using the formula

$$Nu = \frac{C_p m}{A} \quad \frac{(\Delta T_r - Corr)\ \Delta z}{\Delta T\ \lambda\ (1 + \%\ A_{luc}\lambda_{luc}/\lambda)} \qquad (2)$$

where C_p is the specific heat of the cooling fluid (water), m is the mass rate of flow of the cooling fluid, A is the area of the fluid layer,and $\%\ A_{luc}$ is the area of the lucite ring covered by the copper lid divided by the area of the fluid layer. ΔT_r is the temperature difference between the inlet and outlet of the cooling fluid in the heat sensor, and Corr is a correction to ΔT_r accounting for dissipation of the cooling fluid in the heat sensor. This correction is very small, namely of order of $2 \cdot 10^{-3}$°C, but quite important for the value of Nu if the temperature difference applied to the fluid is small and consequently ΔT_r is small. The product C_p m (ΔT_r-Corr) is

the measured value of Qconv+Qcond in formula (1). ΔT in equation (2) is the temperature difference across the fluid layer, λ the thermal conductivity of the fluid, Δz the depth of the fluid layer and A the area of the fluid layer. The product $\lambda \Delta T A/\Delta z$ is Q_{cond} of the fluid layer. The term in parenthesis in the denominator of equation (2) is a correction necessitated by the heat flux through the lucite ring on which the copper lid rests. This correction is of order of % A_{luc} = 5%, because the area covered by the copper lid is 5% of the area of the fluid layer. The thermal conductivities of the silicone oil and the lucite are fairly similar, λ_{luc} being larger than the λ of silicone oil. We use λ_{luc} = 4.17 cal/gm cm sec, which is certainly not more accurate than $\pm$ 10%. We have no information about the variation of λ_{luc} with temperature. The values of the thermal conductivities of the two silicone oils is given later on in equations 5a-b. The parenthesis in the denominator of (2) has then the value 1.056 for the experiments with the 1.0 cm^2/sec silicone oil, and the value 1.069 for the experiments with the 0.1 cm^2/sec silicone oil.

The sum of the uncertainties of all the terms in equation (2) determines the total uncertainty of the Nusselt number, which is about 3% in our experiments, but can be much larger at small values of ΔT because of the correction to ΔT by the dissipation in the heat sensor. The main contributor to the 3% uncertainty is the experimental uncertainty in the determination of ΔT which has, around the critical temperature difference, a standard deviation of $\pm$ 1%. Another percent of the principal uncertainty originated from the uncertainty of the value of the thermal conductivity λ, which is known, at best, with 1% accuracy.

Of the heat flux curves determined we will show here those for the two deepest fluid layers (Fig. 4-5), and those for the two thinnest fluid layers (Fig. 6-7). The curves for the deep layers were made to verify the correct functioning of the apparatus. Fig. 4 shows a practically abrupt break of the heat flux in the 0.501 cm deep layer of 1 cm^2/sec silicone oil at a critical temperature difference of 15.2 $\pm$ 0.1°C. The same can be seen on Fig. 5 showing the heat transfer in the same oil but in a 0.400 cm deep layer. The rounding of the break at ΔT_c = 26.2 $\pm$ 0.2°C is a little more pronounced than in Fig. 4. Other than perhaps through the rounding of the "break" Fig. 5 offers no clue that the motion of the fluid changed from a hexagonal pattern to a roll pattern near onset of convection. The breaks of the heat transfer curves on Figs. 4,5 occur at values of ΔT which agree with the critical temperature differences expected from the visual observations. Fig. 1a was taken at ΔT = 16.0°C and is already supercritical. The very first motions observed in this experiment on the shadowgraph occurred at ΔT = 14.5°C, slightly below ΔT_c on Fig. 4. The critical temperature difference on Fig. 5 is ΔT_c = 26.2°C, in good agreement with ΔT = 26.25°C at which Fig. 2a was taken.

The Nusselt numbers below the critical temperature difference in Figs. 4,5 are not equal to one, as one expects, but slightly smaller, increasing gradually from Nu = 0.96 to Nu = 1. This variation is either an artificial consequence of the value of the correction for the dissipation in the heat sensor, or a consequence of the initial thermal conditions of the apparatus. The correction for the dissipation in the heat sensor has been determined separately in long runs in which ΔT = 0 was approached very slowly. At ΔT = 0 the heat

sensor records the temperature difference generated by dissipation in the cooling fluid. This is a very small signal amounting to 0.00225°C. This value fluctuates by up to 30%, the fluctuations being caused by fluctuations of the cooling water temperature and by electrical noise in the laboratory affecting the emf of the thermopile in the heat sensor. Choosing a different (smaller) value of Corr makes it possible to plot the points for $\Delta T < \Delta T_c$ on a line straddling the value Nu = 1. If dissipation in the heat sensor is not considered (Corr = 0), then the measured points approach Nu = 1 on a line which is above Nu = 1. For consistency we use in Figs. 4-7 the same correction (Corr = 0.00225) since the dissipation in the heat sensor should be independent of the type and depth of the oil in the fluid layer.

Another point to be considered is whether or not the fluid layer was in thermal equilibrium. The thermal relaxation time d^2/κ for the experiments with the 1 cm^2/sec oil is about 250 sec, the relaxation time for the 0.1 cm^2/sec oil is about 50 sec. The heating was increased all 15 minutes so that the temperature increase was 50μV, which corresponds to 1.25°C. So in the 1 cm^2/sec oil more than three relaxation times, and in the 0.1 cm^2/sec oil more than 10 relaxation times elapsed between successive heatings. This should assure thermal equilibrium. Actually since the 0.501 cm deep 1 cm^2/sec silicone oil layer needed the most time for thermal relaxation, the time interval for heating was increased to 20 minutes in this case.

In the thin fluid layers with the 0.1 cm^2/sec silicone oil the heat transfer curves (Fig. 6-7) have breaks at $\Delta T = 21.2 \pm 0.2$°C (Fig. 6) and at $\Delta T = 30.8° \pm 0.2$°C (Fig. 7). The curve in Fig. 7 corre-

sponds to the sequence of pictures shown in Fig. 3a-f, in which experiment, however, the measured temperature differences are larger than on Fig. 7 because of the glass mirror on the bottom of the fluid, while the ΔT's in Fig. 7 have been determined with copper-copper boundaries. Other than the small rounding of the breaks there is again no clue in these two figures that the pattern changes from hexagons to rolls above ΔT_c. Fig. 7 also provides no clue for the existence of the extended range of subcritical motion which we have shown in Figs. 3a-c. The very small increase of Nu between ΔT = 15°C and ΔT_c in Fig. 7 seems to be well within the standard deviation of the measurements, as well as within the uncertainty of the slope of the subcritical section of the heat flux curve caused by the uncertainty of the value of the correction for the dissipation in the heat sensor. Without this correction the subcritical heat flux data are on a line approaching Nu = 1 from above. The failure to pick up the subcritical flow in the heat transfer measurements really does not come as a surprise since the motions were so weak that it was difficult to visualize them. The subcritical motions are obviously so slow that the amount of additional heat transferred by them is too small to be measured with our equipment. We have, likewise, not been able to pick up a signal for the increase of the heat transfer by subcritical rolls induced by the lateral wall in earlier Rayleigh-Benard convection experiments (Koschmieder and Pallas, 1974).

3.3 Critical Rayleigh Numbers

From the critical temperature differences determined by the heat flux measurements follow the critical Rayleigh numbers, using the formula

$$R_c = \frac{\alpha g \Delta T_c d^3}{\nu \kappa} \qquad (3)$$

where α is the volume expansion coefficient of the fluid, g the acceleration of gravity, ΔT_c the critical temperature difference, d the depth of the fluid, ν the kinematic viscosity, and κ the thermal diffusivity of the fluid. The value of the critical Rayleigh number of a Boussinesq fluid layer on an infinite plane is $R_c = 1708$. Determining the value of R_c in our experiments is important so that we can compare our results with the theoretical predictions about the onset of convection in non-Boussinesq fluid layers.

In order to use (3) one has to know the material properties α, ν and κ of the fluid, and their dependence on temperature. The volume expansion coefficients of both fluids used (Dow Corning, 200 Fluid) are independent of temperature over the range of temperature considered, and have according to the manufacturer the values $\alpha = 0.00096\ (°C)^{-1}$ for the 1 cm^2/sec oil, and $\alpha = 0.00108\ (°C)^{-1}$ for the 0.1 cm^2/sec oil. The kinematic viscosity is the property that changes most with temperature. According to McGregor (1954) the kinematic viscosity of the silicone oils has the smallest temperature slope of all organic oils. The relationship for the decrease of ν with temperature is

$$\log \nu = \frac{722.5}{T_m} + \frac{0.00032}{T_m} \cdot \nu_1 + 1.004 \log \nu_1 - 2.447$$

where T_m is the mean temperature of the fluid layer and ν_1 the viscosity of the fluid at 25°C. For the 1 cm^2/sec silicone oil the viscosity varies from 1.0 cm^2/sec at 25°C to 0.66 cm^2sec at 50°C mean temperature. For the 0.1 cm°/sec oil the viscosity varies from 0.1 cm^2/sec at 25°C to 0.062 cm^2/sec at 50°C mean temperature.

The viscosity of the fluids which we used have been checked by us because the fluids had been stored in the laboratory for a couple of years. For the determination of the viscosity of the (nominal) 1.0 cm^2/sec oil we used a Contraves Low Shear viscometer, as well as a Brookfield Syncroelectric viscometer. For the nominal 0.1 cm^2/sec oil we used three viscometers, the Contraves, the Brookfield, and the capillary Cannon-Finske viscometer. The results of these viscosity measurements were disappointing, there were significant differences in the values of the viscosity of one and the same fluid at the same temperature when measured with different instruments. There was a deviation of about 10% between the lowest and highest value of the viscosity. To eliminate operator error the viscosity measurements have been made independently by two people, the consistency of their results was excellent being within less than 1%. A decision had to be made which of the measured viscosities was most likely correct. This decision was based on the assumption that the instrument that measured brand new silicone oil of nominal 1.0 cm^2/sec viscosity at 1.00 ± 0.01 cm^2/sec was indeed working correctly. The viscosity of the old nominal 1.0 cm^2/sec oil was then determined to be $\nu = 1.079 \pm 0.005$ cm^2/sec at 25°C, the error quoted being the standard deviation of the measurements, not the principal uncertainty. For the 0.1 cm^2/sec oil the Contraves and Brookfield viscometers use spindles different from those used with 1.0 cm^2/sec fluids, which make the consideration above irrelevant. For this viscosity measurement the capillary viscometer was used as the norm because a calibration fluid was available for this instrument. The reading of the instrument agreed within 1.5% with the viscosity of the calibration fluid. The viscosity of the old

0.1 cm^2/sec (nominal) silicone oil was so determined to be 0.102 $\pm$ 0.001 cm^2/sec at 25°C, the error being again the standard deviation of the measurements with this instrument.

The thermal diffusivity κ follows from the formula $\kappa = \lambda/\rho c_p$ where λ is the thermal conductivity, ρ the density and c_p the specific heat. Values of λ have been given by the manufacturer at 50°C and 80°C, from which one has to extrapolate to room temperature. In the range of temperatures considered we have used linear approximations which are

$$\lambda = (4.325 - 0.013\ T_m)\cdot 10^{-4}\ cal/cm\ sec\ °C \qquad (5a)$$

and $$\lambda = (3.2233 - 0.00166 T_m)\cdot 10^{-4}\ cal/cm\ sec\ °C \qquad (5b)$$

for the 1.0 cm^2/sec oil and for the 0.1 cm^2/sec oil respectively. There is certainly a principal error in these values of order of 1% or even more. We will see that the thermal conductivity can, however, be assessed from the subcritical part of the heat transfer curves, and that within about 1% the thermal conductivities given in (5a), (5b) are correct. The density ρ of the fluid varies linearly with the expansion coefficient, for the 1.0 cm^2/sec oil at 25°C it is for example $\rho = 0.960\ gm/cm^3$, and for the 0.1 cm^2/sec oil ρ at 25°C is $\rho = 0.934$. The specific heat c_p is also a linear function of temperature. For the 1.0 cm^2/sec oil c_p is for example $c_p = 0.381$ cal/gm at 25°C, and for the 0.1 cm^2/sec oil it is $c_p = 0.392$ cal/gm at 25°C. The value of κ of the 1.0 cm^2/sec oil is then $\kappa = 0.00109\ cm^2/sec$ at 25°C, and for the 0.1 cm^2/sec oil $\kappa = 0.00087\ cm^2/sec$ at 25°C.

The cumulative uncertainty in the experimental value of R_c is determined mainly by the uncertainty of ΔT_c, d^3, ν and κ. ΔT_c is determined from the heat flux curves. The intersection of the subcritical

part of the heat flux curves with the supercritical part of the heat flux curves is certainly not known with an error less than $\pm$ 1%, which is also the average magnitude of the standard deviation of the measurements of the Nusselt numbers of the points which make up the heat flux curves. It is therefore optimistic to ascribe to ΔT_c an error of only $\pm$ 1%. We measure the depth of the fluid layer with an accuracy of about 10^{-2}mm, so the uncertainty of d^3 is on the average, about $\pm$ 1%. We believe that the uncertainty in ν is of order of 2%, if not more. The uncertainty in the value of κ, which involves the cumulative uncertainty of λ, ρ,and c_p, is also of order 2%. The cumulative uncertainty of R_c is then of order of $\pm$ 6%.

The values of R_c determined from the measured ΔT_c are listed in Table 1, together with the depth of fluid layers and the critical temperature differences. The depth 0.210 cm is listed twice, and the second case is marked c. This refers to control experiments done at this depth with a brand new sample of silicone oil of 0.1 cm^2/sec viscosity. These control experiments were done because of the uncertainty of the value of the viscosity of the fluids. Table 1 also has a column listing values of λ_t/λ, which column deals with the thermal conductivity of the fluids as it follows from the subcritical part of the heat flux curves. This item will be discussed first.

As mentioned before in connection with equation (2) the heat conducted through the apparatus by the resting fluid is proportional to the term $(1 + \% A\lambda_{luc}/\lambda)$. This term is the ratio of the total thermal conductivity λ_t of the fluid and the lucite rim to the conductivity λ of the fluid only. The experimental value of λ_t/λ follows from the requirement that the Nusselt number should be equal to one in the sub-

critical part of the heat flux curve or at least equal to one just before ΔT_c. The values of λ_t/λ necessary to satisfy this requirement are listed in Table 1. The following column lists the deviation Δ of the experimental values from the values to be expected from (1 + % $A\lambda_{luc}/\lambda$). As mentioned in context with equation (2) the term λ_t/λ = (1 + % $A\lambda_{luc}/\lambda$) is = 1.056 for the 1 cm^2/sec oil, and = 1.069 for the 0.1 cm^2/sec oil. The actual value of λ_t/λ varies slightly because λ is a function of temperature, as is λ_{luc}; but this is of little significance. As can be seen in Table 1 the deviation Δ is in most cases positive. A positive deviation means that more heat is conducted than expected. This can be caused by a thermal conductivity of the fluid which is larger than the conductivity we have used in the calculation of λ_t/λ. Note, however, that then all layers with the same fluid are affected in the same way. A positive Δ can also be caused by additional heat being conducted to the copper lid by portions of the lucite rim not being covered by the lid, in other words, by an apparent increase of % A. A positive Δ can, furthermore, be caused by a fluid layer with a depth smaller than the depth used in the calculations; the depth of the layer is not known with an accuracy better than $\pm$ 1%. Negative deviations Δ mean that the heat flux is smaller than expected, which can be caused by a fluid depth larger than the depth we have used. This seems to be most applicable to the experiment with 0.163 cm depth. In all, the deviations of λ_t/λ are not more than $\pm$ 2% and confirm with that accuracy the thermal conductivities given by equations 5 a-b. This is important because it means that the critical Rayleigh numbers cannot be affected by more than $\pm$ 2% by uncertainties of the value of the thermal conductivity.

Finally, we discuss the critical Rayleigh numbers. The column R_c in Table 1 lists the values of the R_c determined from our experiments. The errors listed are the 6% of the R_c which are the principal uncertainty of the measurements of R_c as discussed before. As is apparent the values of R_c fall into two categories, namely values of around 1800 ± 100 for the two deep fluid layers with the 1.0 cm^2/sec oil, and values of around 2200 ± 130 for the four thinner fluid layers with the 0.1 cm^2/sec oil. The column R_c/R_{ctheor} shows how far the measured R_c differ from the theoretical value $R_{ctheor} = 1708$. While the values of R_c for the two deep fluid layers are larger than R_{ctheor}, they are within the experimental uncertainty still compatible with R_{ctheor}. The conditions in the two deep layers are already non-Boussinesq, the degree of viscosity variation can be seen from the last column of Table 1, where the ratio of the maximal viscosity in the fluid layer, (namely in the fluid just under the lid), to the minimal viscosity in the fluid, (namely in the fluid at the bottom), is listed. Although the experimental values of R_c for the two deep layers are still compatible with R_{ctheor}, they raise questions about the validity of the concept that the onset of convection in non-Boussinesq fluid layers takes place as a subcritical bifurcation at a value of R smaller than R_{ctheor}.

The experimental critical Rayleigh numbers in the thin fluid layers are all clearly above 1708 by about 30%, with no recognizable trend with regard to either depth or viscosity ratio. In order to check on the startling value of R_c the experiments with the 0.210 cm deep layer have been repeated with brand new silicone oil of 0.1 cm^2/sec viscosity (nominal), in order to eliminate any possible conse-

quence originating from the use of one particular sample of the oil. As Table 1 shows the R_c measured with the new oil fits right in with the previous results, so there is no particular property of the old oil that affected the outcome of the experiments. A 30% deviation of the critical Rayleigh number from the value of 1708 appears to be outside of the experimental error. We have mentioned above that we have ascertained that the thermal conductivity of the fluid cannot vary more than $\pm$ 2% from the values which follow from (5a,b). We have mentioned the possibility of a substantial uncertainty in the value of the kinematic viscosity. However, the value of ν of the 0.1 cm^2/sec oil is not only the value suggested by the manufacturer, but also the value of ν determined with the capillary viscometer. This instrument is best suited for the measurement of small viscosities, and the accuracy of this viscometer has been verified with the calibration fluid. Assuming that the largest discrepancy of the viscosity measurements, which was + 10%, would actually be a correct viscosity, then that would still not reduce our experimental R_c to a value compatible with 1708. It does not appear that the other material properties or ΔT_c contribute an error sufficiently large in order to explain our value of R_c. We conclude, therefore, that the experimental value of R_c is indeed <u>above</u> R_c = 1708, contradicting thereby theories that place the onset of convection in slightly non-Boussinesq fluid layers at values of $R < 1708$. We note, on the other hand, that the theory of Stengel, Oliver and Booker (1982) predicts that the onset of convection in strongly non-Boussinesq fluid layers occurs at $R > 1708$. Our results confirm this finding, although we work with viscosity variations not nearly as large as those considered by Stengel et al.

4. Conclusions

Our experiments have two essential results. First, we have found that in thin fluid layers the onset of Rayleigh-Benard convection is preceded by subcritical convective motions. Secondly, we have found that the onset of Rayleigh-Benard convection in non-Boussinesq fluid layers takes place in the form of hexagonal cells at Rayleigh numbers larger than the critical Rayleigh number R_c = 1708 which determines the onset of convection in Boussinesq fluid layers.

Concerning our first finding, namely the observation of the subcritical motions, these occur only if the fluid is sufficiently thin, of order of 2 mm or less. The thinner the fluid is the larger is the range of occurrence of subcritical motions. There is apparently no critical value of the temperature difference for the appearance of the subcritical flow, the motions form with barely observable amplitude which increases very slowly as the temperature difference is increased. This is followed by a spectacular spontaneous amplification of the amplitude of the flow at the genuine onset of convection, which becomes apparent as an enormous multiplication of the intensity of light on the shadowgraph. The search for subcritical motions was the motif for our experiments and originated from the unexpected appearance of subcritical motions in the Benard convection experiments of Koschmieder and Biggerstaff (1986). Observing subcritical motions also in Rayleigh-Benard convection confirms what we found in the Benard convection experiments, in which surface tension gradients seem to amplify the subcritical motions, they were much more easily observable under an air surface than in the Rayleigh-Benard experiments. Our observations in the current experiments have shifted the search

for the explanation of the subcritical flow in Benard convection to a search for an explanation for the subcritical motions in Rayleigh-Benard convection. We will not speculate here about the cause of the subcritical motions.

It appears that subcritical motions in thin fluid layers heated uniformly from below are a principal feature, not an avoidable consequence of an experimental deficiency. We are led to believe this by the significant differences in the horizontal boundary conditions of the fluid under which we have observed subcritical flow. We have observed subcritical flow with either an air surface in Koschmieder and Biggerstaff (1986) or here with the sapphire on top of the fluid. This involves the differences between near slip and no slip conditions, as well as the change from very poor thermal conduction to very good thermal conduction. On the bottom of the fluid we have had the copper block, or the steel mirror or the glass mirror. That again involves the very large changes in thermal conductivity between the copper block and the glass mirror, as well as changes in the smoothness of the bottom, being only good with the copper but excellent with the glass mirror; while the smoothness of the top boundary of the fluid was excellent with either the air surface or the sapphire. We believe that influences of the lateral wall are minimal because the lateral wall is made of a very poor thermal conductor and the aspect ratio of the fluid layer is very large ($\Gamma \simeq 60$). We note, furthermore, that the range of subcritical motions increases as the influence of the lateral wall decreases with ever thinner fluid layer or increased aspect ratio. The decisive feature for the occurence of subcritical flow seems to be the small depth of the fluid layer.

Concerning the question of the onset of Rayleigh-Benard convection in non-Boussinesq fluid layers, we are faced there with a dilemma. We can confirm quite clearly the long-standing theoretical predictions that the onset of convection in this case should take place in the form of hexagonal cells which transform into rolls at slightly higher Rayleigh numbers. While the theories predict the pattern and the change of the pattern correctly we come, however, to a contradiction with the same theories when we look at the Rayleigh number at which the onset of convection occurs. We find that onset of convection takes place at Rayleigh numbers larger than $R_c = 1708$, while the theories predict that the hexagonal cells form at Rayleigh numbers smaller than $R_c = 1708$. Only the most recent theoretical investigation of convection in non-Boussinesq fluid layers (Stengel, Oliver and Booker, 1982) places the onset of convection at values of $R>R_c$, provided that the viscosity variation in the fluid layer is very large. It is necessary to first clarify the theory with regard to the point whether or not the onset of convection in non-Boussinesq fluid layers occurs at Rayleigh numbers larger or smaller than $R_c = 1708$ before a conclusion can be drawn as to whether our experimental findings are in agreement with theory.

Help of Professor R. S. Schechter is gratefully acknowledged. We thank Mr. T. H. Koschmieder for programming the data evaluation. Support of this work through the National Aeronautics and Space Agency is also gratefully acknowledged.

Table 1

d (cm)	ΔT_c (°C)	λ_t/λ	Δ %	R_c	R_c/R_{ctheor}	ν_{max}/ν_{min}
0.501	15.3	1.082	+2.5	1819±109	1.065	1.31
0.400	26.2	1.073	+1.6	1776±107	1.040	1.57
0.221	14.2	1.081	+1.2	2196±132	1.286	1.29
0.210	16.6	1.058	-1.0	2284±137	1.337	1.34
0.210c	15.9	1.082	+1.3	2258±136	1.322	1.33
0.187	21.6	1.077	+0.8	2175±130	1.274	1.46
0.163	30.8	1.045	-2.2	2240±134	1.311	1.69

References

Busse, F. H. 1967 J. Fluid Mech. 30, 625-649.

Davis, S. H. & Segel, L. A. 1968 Phys. Fluids 11, 470-476.

Hoard, C. Q., Robertson, C. R. & Acrivos, A. 1970 Intl. J. Heat Mass Transfer 13, 849-856.

Jenkins, D. R. 1986 J. Fluid Mech. Submitted.

Koschmieder, E. L. 1966 Beitr. Phys. Atmos. 39, 1-11.

Koschmieder, E. L. & Pallas, S. G. 1974 Intl. J. Heat Mass Transfer 17, 991-1002.

Koschmieder, E. L. & Pallas, S. G. Rev. Sci. Instrum. 45, 1164-1165.

Koschmieder, E. L. & Biggerstaff, M. I. 1986 J. Fluid Mech. 167, 49-64.

McGregor, R. R. 1954 Silicones and Their Uses, McGraw-Hill, New York.

Oliver, D. S. & Booker, J. R. 1983 Geophys. Astrophys. Fluid Dynamics 27, 73-85.

Palm E. 1960 J. Fluid Mech. 8, 183-192.

Palm E., Ellingsen, T. & Gjevik, B. 1967 J. Fluid Mech. 30, 651-661.

Schmidt, R. J. & Milverton, S. W. 1935 Proc. R. Soc. A 152, 586-594.

Silveston, P. L. 1958 Forsch. Ing. Wes. 24, 29-32, 59-69.

Stengel, K.C., Oliver, D. S. & Booker, J. R. 1982 J. Fluid Mech. 120, 411-431.

Segel, L. A. & Stuart, J. T. 1962 J. Fluid Mech. 13, 289-306.

Figure Captions

Fig. 1a. Shadowgraph pictures of convection in the form of circular concentric rolls at ΔT = 16.0°C = 1.10 ΔT_c in the 5.01 mm deep layer of silicone oil of 1.0 cm^2/sec viscosity. The steel mirror is at the bottom, the sapphire on top of the fluid.

Fig. 1b. Convection in circular concentric rolls in the 5.01 mm deep layer at ΔT = 1.64 ΔT_c. The diameter of the innermost ring has shrunk.

Fig. 1c. Convection in circular concentric rolls in the 5.01 mm deep layer at ΔT = 2.33 ΔT_c. The original innermost ring has been reduced to a point by the increase of the wavelength of the motion.

Fig. 2a. Onset of convection in the 4.00 mm deep layer of silicone oil of 1.0 cm^2/sec viscosity at ΔT = 26.25°C = ΔT_c. The pattern is cellular in a circular arrangement. Steel mirror - sapphire boundaries.

Fig. 2b. Circular concentric rolls in the 4.00 mm deep layer at ΔT = 1.05 ΔT_c. The cells have disappeared.

Fig. 3a. Shadowgraph picture of subcritical convective motions in the 1.63 mm deep layer of 0.10 cm^2/sec viscosity at ΔT = 28.75 °C = 0.74 ΔT_c. A glass mirror is at the bottom, the sapphire on top of the fluid.

Fig. 3b. Subcritical flow in the 1.63 mm deep layer at ΔT = 0.84 ΔT_c.

Fig. 3c. Subcritical flow in the 1.63 mm deep layer at ΔT = 0.90 ΔT_c.

Fig. 3d. Critical cellular flow in the 1.63 mm deep layer at ΔT = 38.75°C = ΔT_c.

Fig. 3e. Beginning of the transformation of the cellular pattern into a roll pattern. 1.63 mm deep layer, $\Delta T = 1.03\ \Delta T_c$.

Fig. 3f. Supercritical flow in the 1.63 mm deep layer. The transformation of the pattern into rolls is nearly completed.

Fig. 4. Heat transfer in the 5.01 mm deep layer of silicone oil of 1 cm^2/sec viscosity. Copper - copper boundaries. Only three characteristic error bars have been plotted.

Fig. 5. Heat transfer in the 4.00 mm deep layer of silicone oil of 1 cm^2/sec viscosity. Copper - copper boundaries.

Fig. 6. Heat transfer in the 1.87 mm deep layer of silicone oil of 0.10 cm^2/sec viscosity. Copper-copper boundaries.

Fig. 7. Heat transfer in the 1.63 mm deep layer of silicone oil of 0.10 cm^2/sec viscosity. Copper - copper boundaries.

Table 1. Critical temperature differences, thermal conductivities, Rayleigh numbers and viscosity variations for the different fluid layers.

Table 1

d (cm)	ΔT_c (°C)	λ_t/λ	Δ %	R_c	R_c/R_{ctheor}	ν_{max}/ν_{min}
0.501	15.3	1.082	+2.5	1819±109	1.065	1.31
0.400	26.2	1.073	+1.6	1776±107	1.040	1.57
0.221	14.2	1.081	+1.2	2196±132	1.286	1.29
0.210	16.6	1.058	-1.0	2284±137	1.337	1.34
0.210c	15.9	1.082	+1.3	2258±136	1.322	1.33
0.187	21.6	1.077	+0.8	2175±130	1.274	1.46
0.163	30.8	1.045	-2.2	2240±134	1.311	1.69

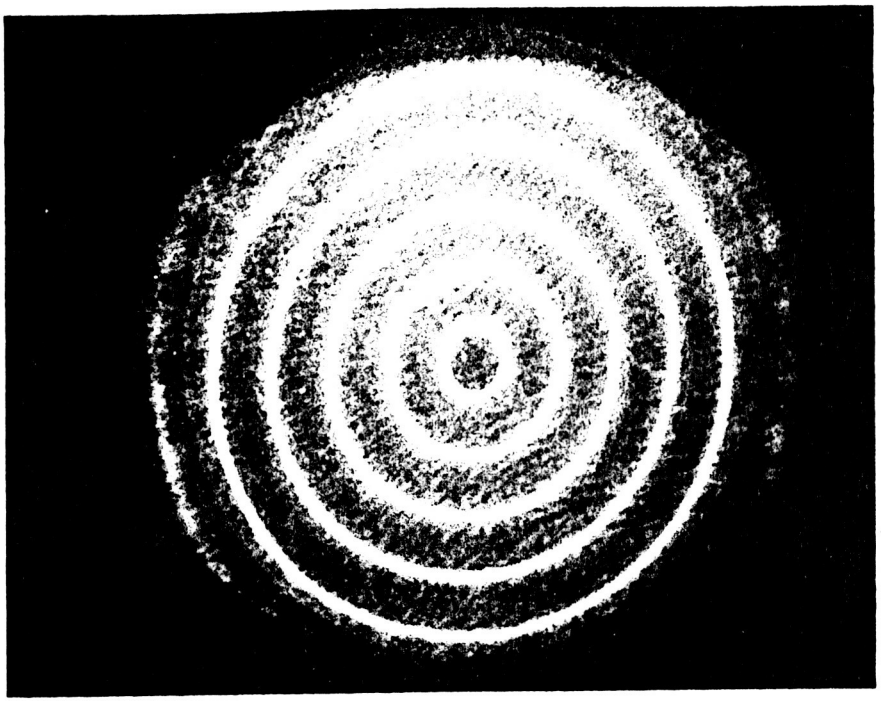

Fig. 1a

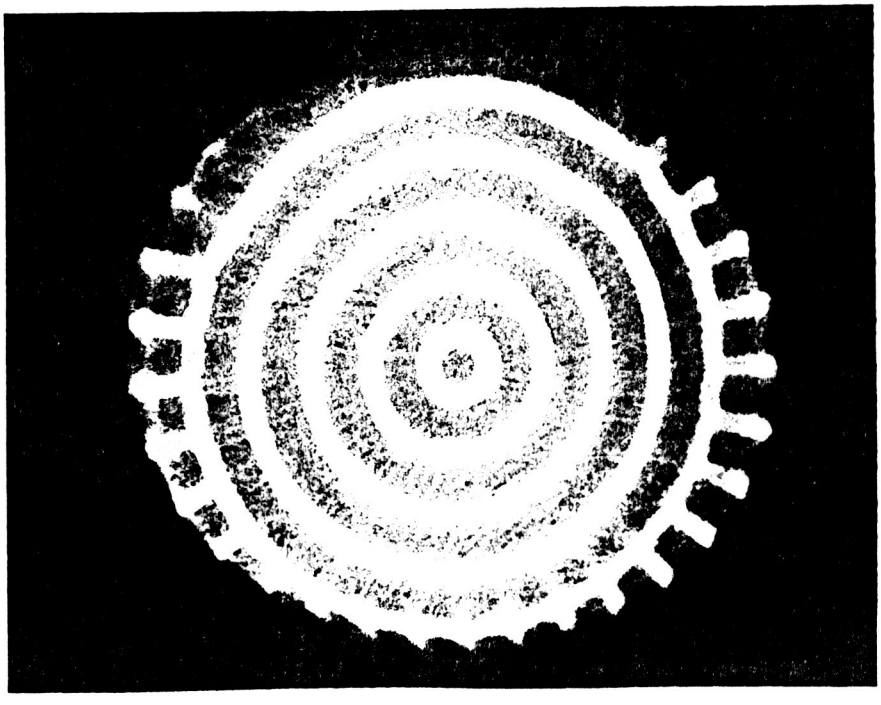

Fig. 1b

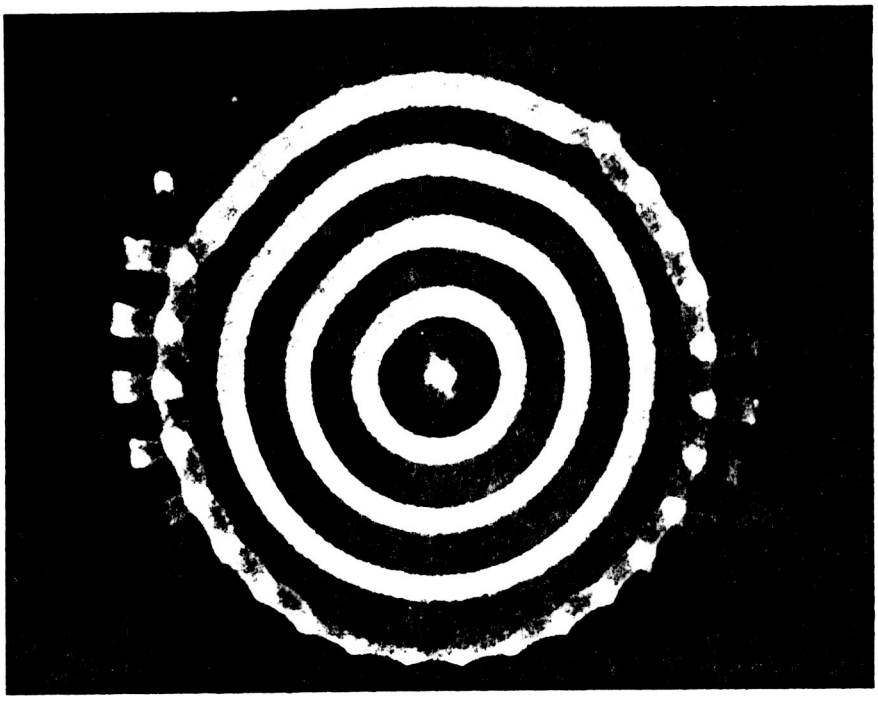

Fig. 1c

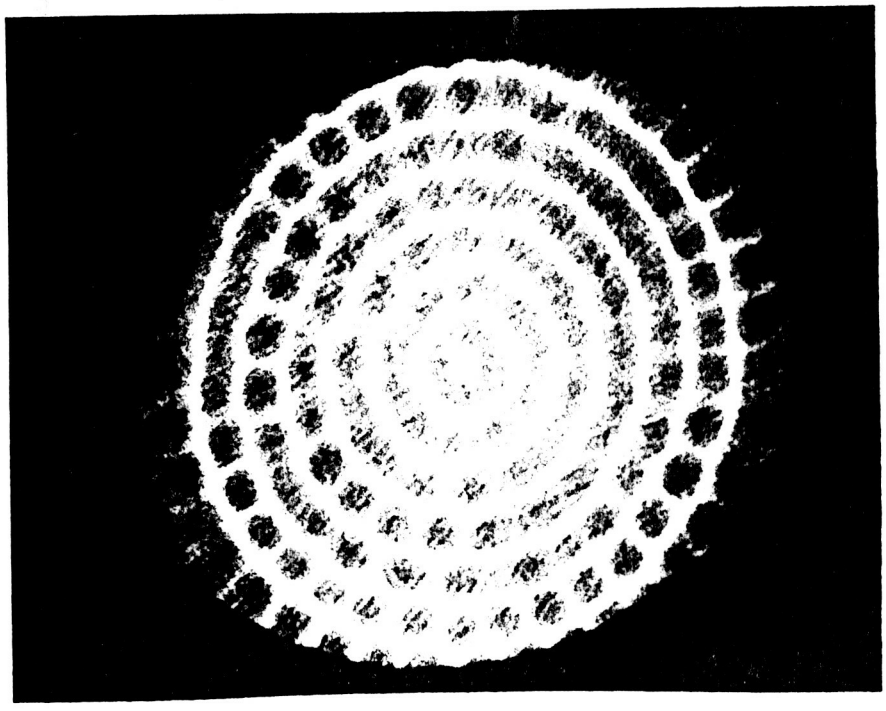

Fig. 2a

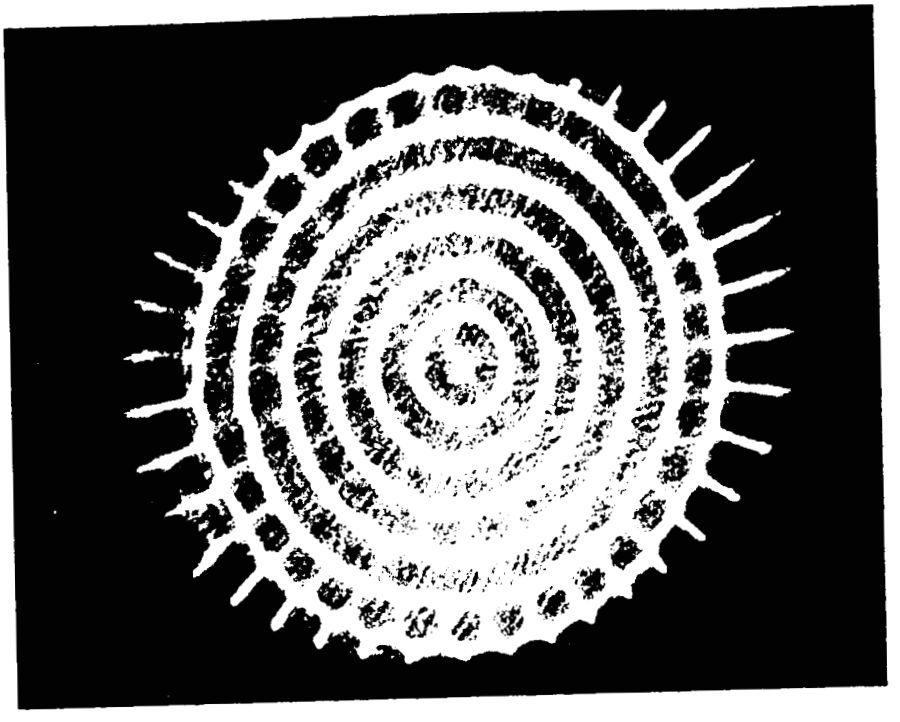

Fig. 2b

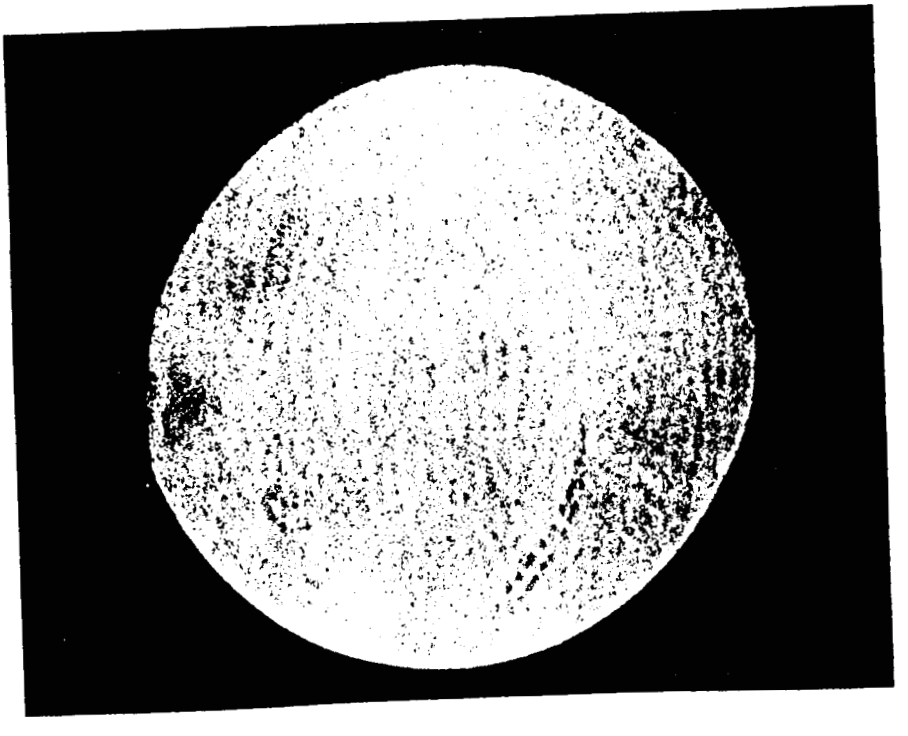

Fig. 3a

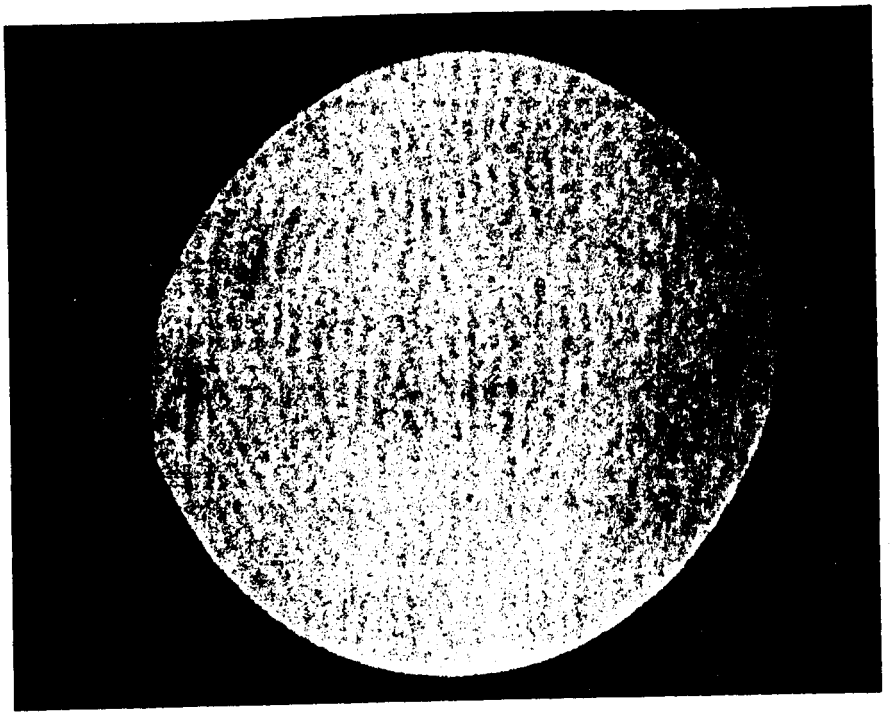

Fig. 3b

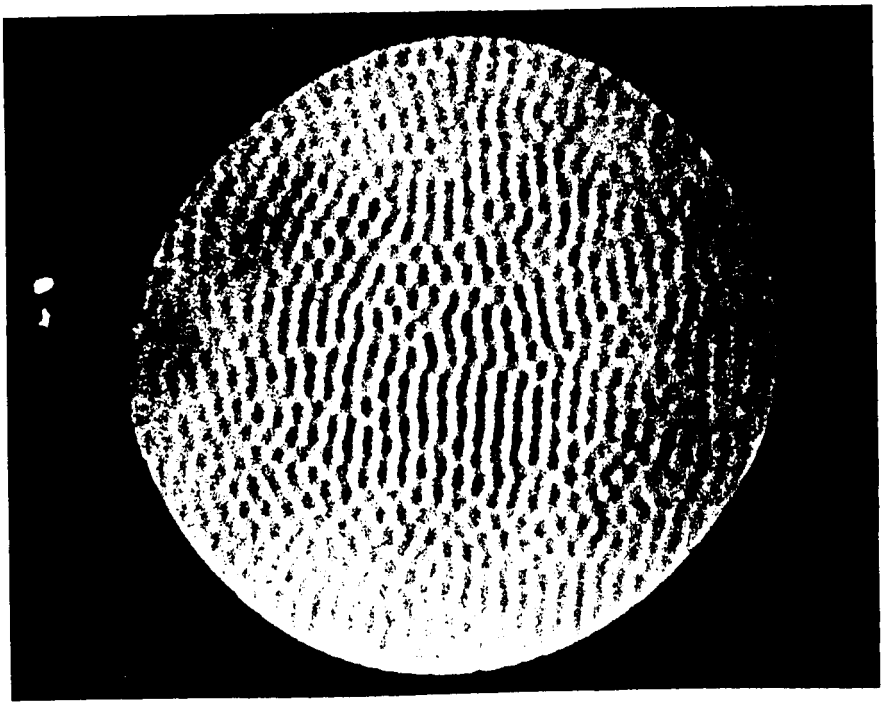

Fig. 3c

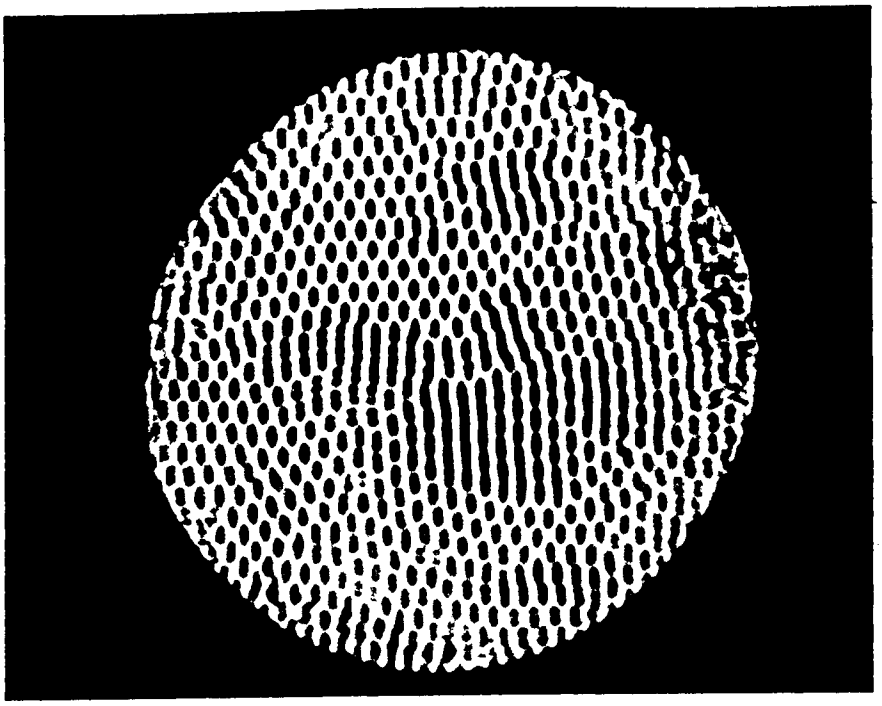

Fig. 3d

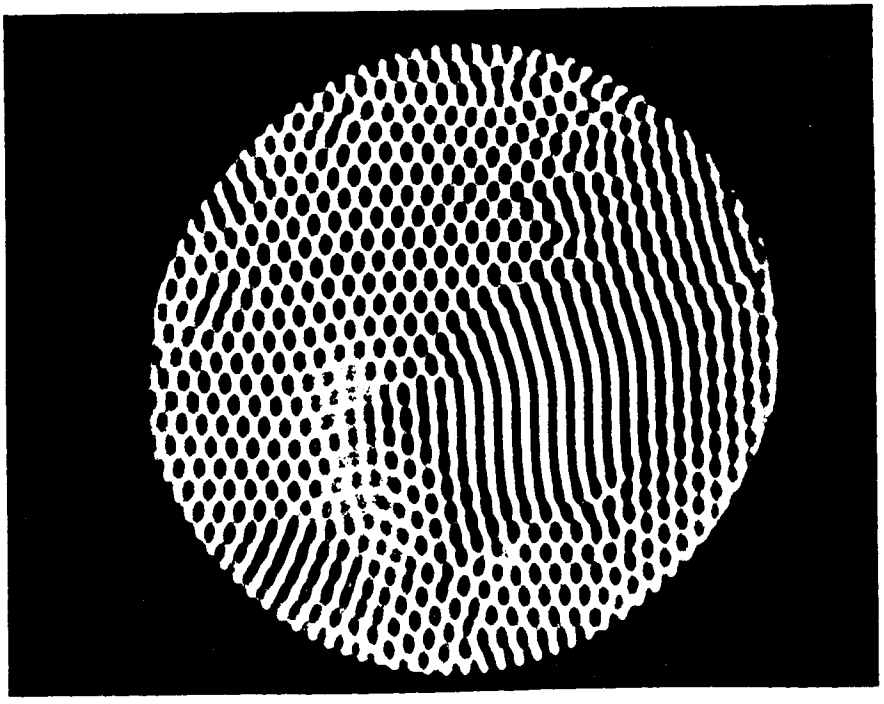

Fig. 3e

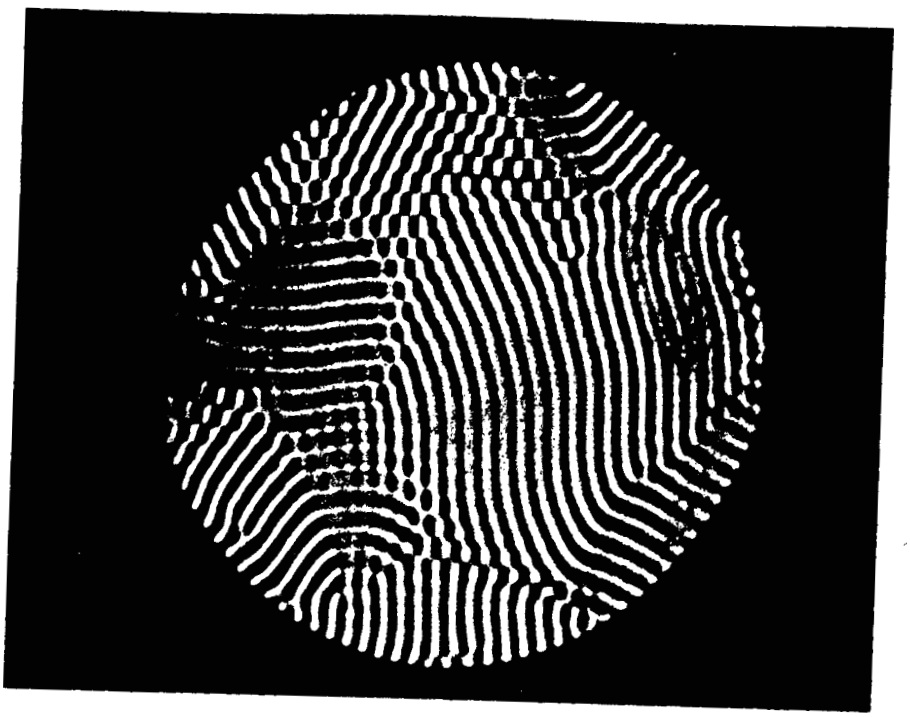

Fig. 3f

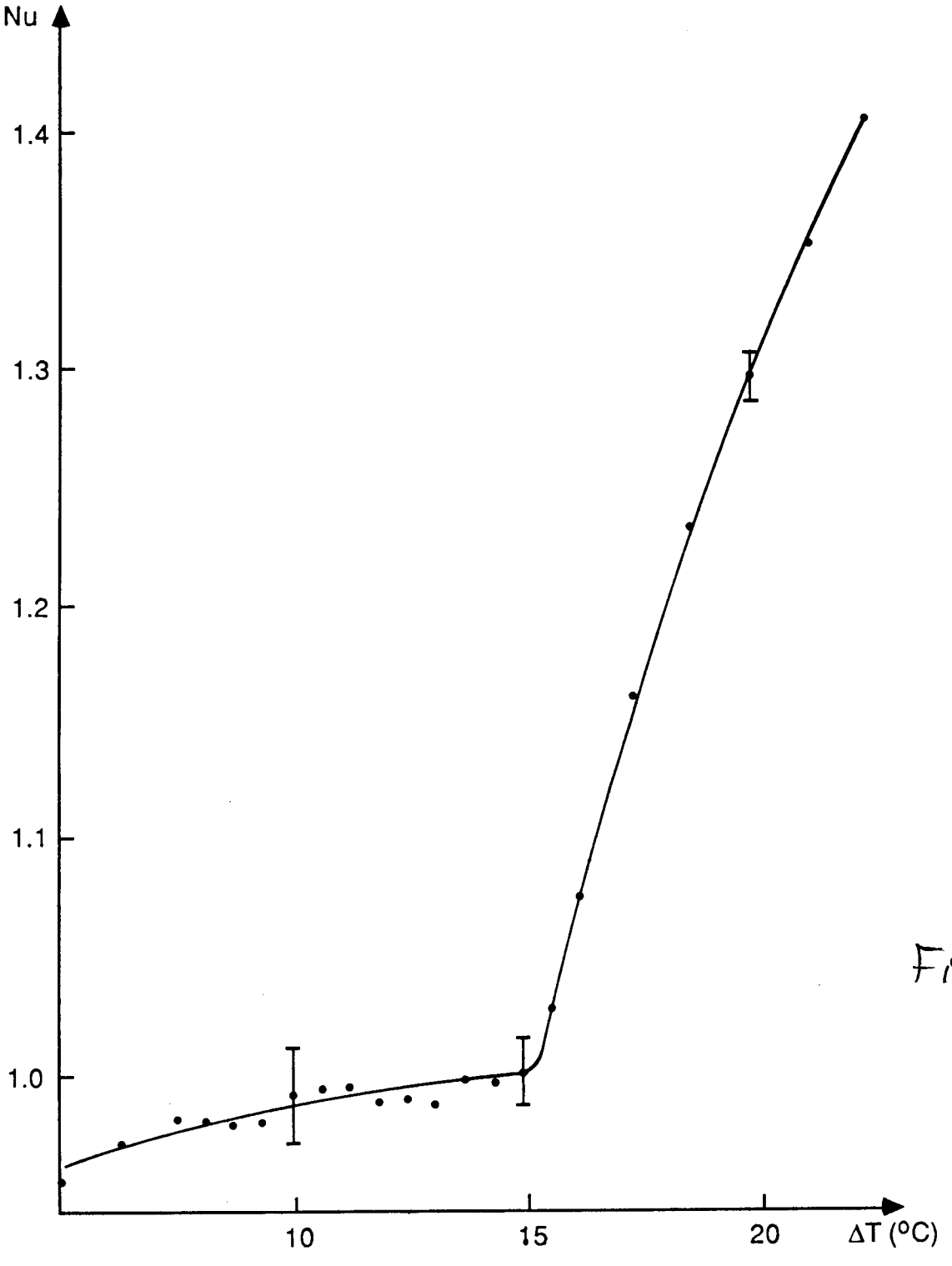

Fig. 4

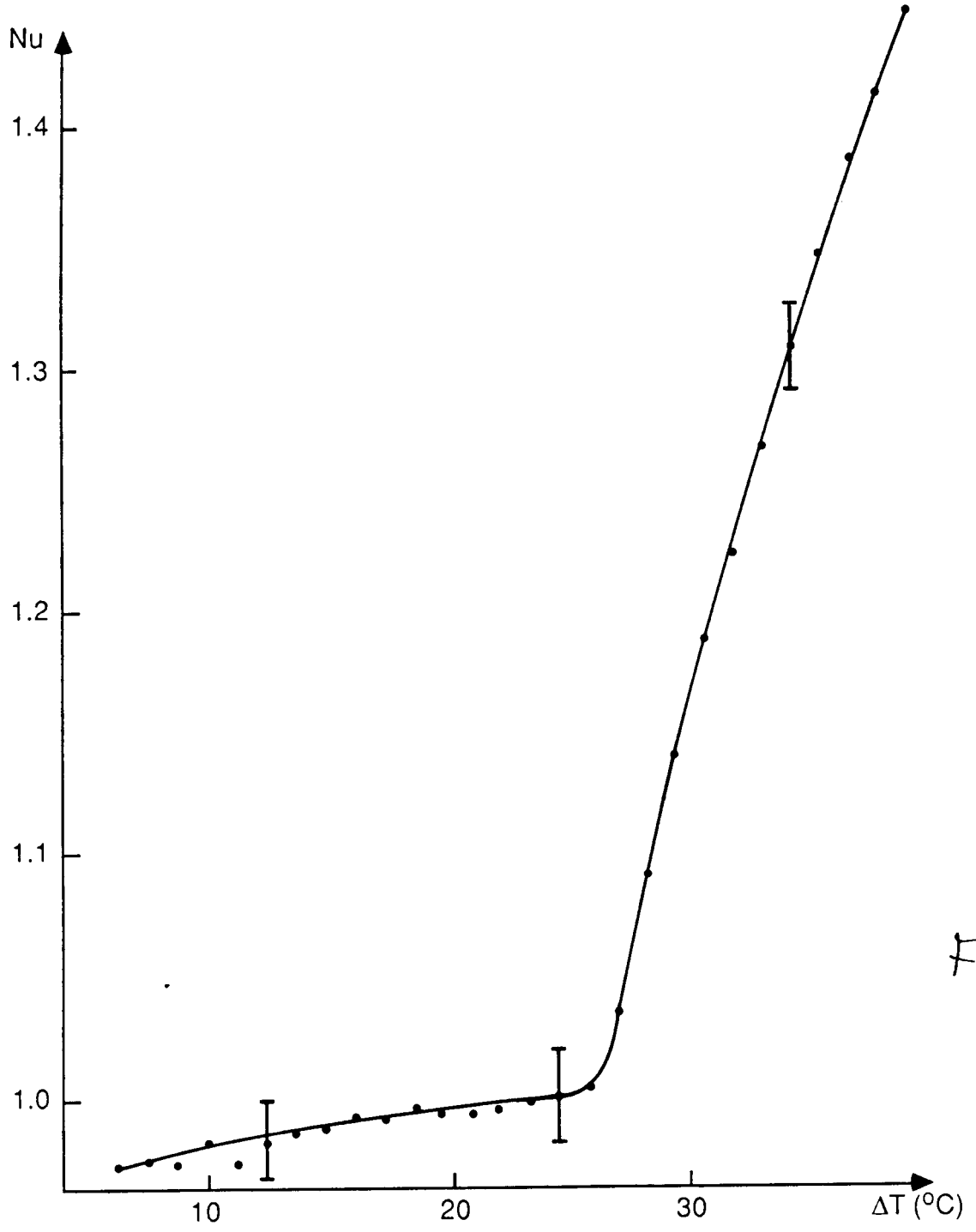

Fig. 5

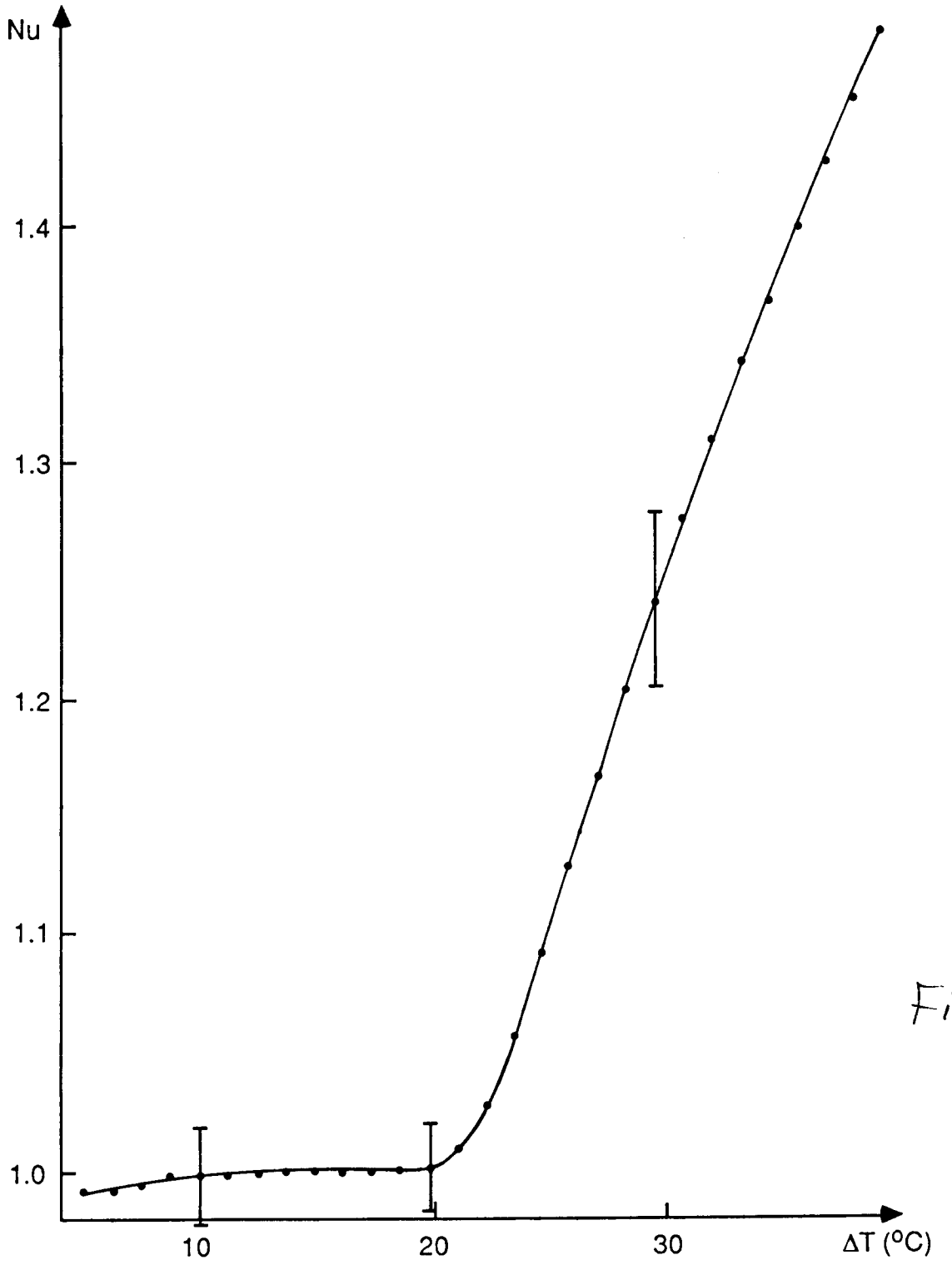

Fig. 6

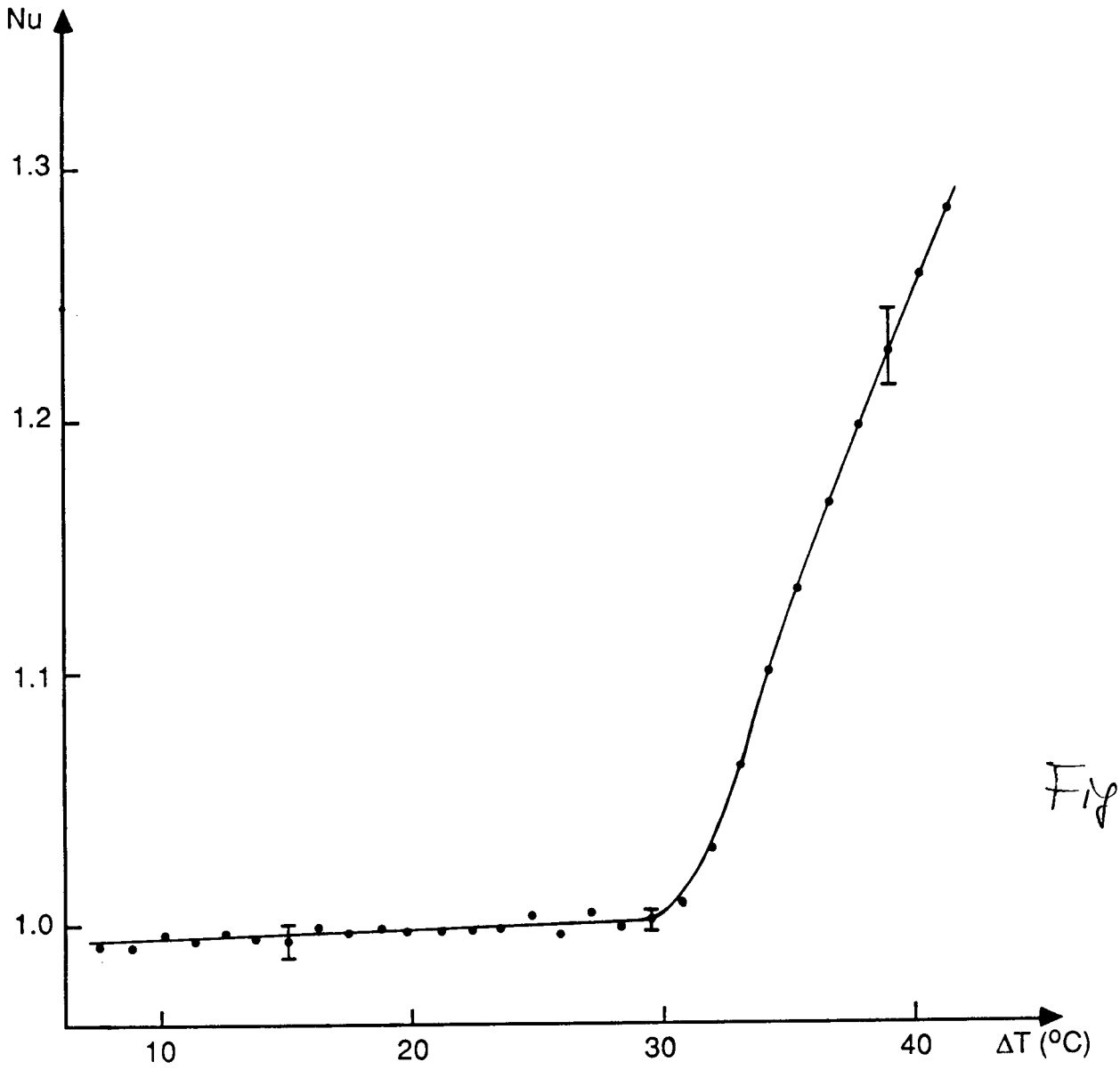

Fig. 7